ERDC TR-14-7

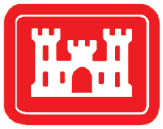

US Army Corps
of Engineers®
Engineer Research and
Development Center

Three-Dimensional Shallow-Water Adaptive Hydraulics (ADH-SW3): Hydrodynamic Verification and Validation

Gaurav Savant, R. Charlie Berger, Tate O. McAlpin,
and Corey J. Trahan

September 2014

Engineer Research and Development Center

The US Army Engineer Research and Development Center (ERDC) solves the nation's toughest engineering and environmental challenges. ERDC develops innovative solutions in civil and military engineering, geospatial sciences, water resources, and environmental sciences for the Army, the Department of Defense, civilian agencies, and our nation's public good. Find out more at www.erdc.usace.army.mil.

To search for other technical reports published by ERDC, visit the ERDC online library at http://acwc.sdp.sirsi.net/client/default.

ERDC TR-14-7
September 2014

Three-Dimensional Shallow-Water Adaptive Hydraulics (ADH-SW3): Hydrodynamic Verification and Validation

Gaurav Savant

Dynamic Solutions LLC
6421 Deane Hill Dr., Suite 1
Knoxville, TN 37919

R. Charlie Berger and Tate O. McAlpin

Coastal and Hydraulics Laboratory
U.S. Army Engineer Research and Development Center
3909 Halls Ferry Rd.
Vicksburg, MS 39180

Corey J. Trahan

Information Technology Laboratory
U.S. Army Engineer Research and Development Center
3909 Halls Ferry Rd.
Vicksburg, MS 39180

Final report

Prepared for U.S. Army Corps of Engineers
Washington, DC 20314-1000

Abstract

The U.S. Army Engineer Research and Development Center (ERDC), Coastal and Hydraulics Laboratory (CHL), has undertaken the development of the multi-module Adaptive Hydraulics (ADH) hydrodynamic, sediment, water quality and transport numerical code. As a natural progression of this development process, verification of ADH was performed to known solutions for the basic physics contained in the numerical code. This report documents verification and validation of the model performed by applying the model to several analytic and flume experiments. These tests were designed to ensure that the ADH-SW3 is solving the pertinent equations accurately.

Contents

Figures and Tables

Figures

Tables

Preface

This report represents the findings of the ADH-SW3 verification and validation efforts. ADH-SW3 demonstrates the ability to accurately and adequately represent hydrodynamics as well as associated baroclinic transport phenomenon in a stratified environment associated with navigation channels, reservoirs, etc.

This investigation was conducted from January 2012 through December 2013 at the U.S. Army Engineer Research and Development Center (ERDC) by Dr. Gaurav Savant of Dynamic Solutions LLC, Tate O. McAlpin and Dr. R.C. Berger of the Coastal and Hydraulics Laboratory (CHL), and Dr. Corey J. Trahan of the Information Technology Laboratory (ITL). Funding was provided by the Flood and Coastal Storm Damage Reduction Program of the U.S. Army Corps of Engineers.

The work was performed under the general direction of José Sánchez, Director, CHL; Dr. Ty V. Wamsley, Chief, Flood and Storm Protection Division; and Dr. Robert McAdory, Chief, Estuarine Engineering Branch, CHL.

At the time of publication of this report, Dr. Jeffery P. Holland was Director of ERDC, and COL Jeffrey Eckstein was Commander and Executive Director.

Unit Conversion Factors

Multiply	By	To Obtain
cubic feet	0.02831685	cubic meters
cubic yards	0.7645549	cubic meters
degrees (angle)	0.01745329	radians
feet	0.3048	meters
knots	0.5144444	meters per second
microns	1.0 E-06	meters
miles (nautical)	1,852	meters
miles (U.S. statute)	1,609.347	meters
miles per hour	0.44704	meters per second
pounds (force)	4.448222	newtons
slugs	14.59390	kilograms
square feet	0.09290304	square meters
square miles	2.589998 E+06	square meters
square yards	0.8361274	square meters
yards	0.9144	meters

1 Introduction

The U.S. Army Corps of Engineers (USACE), through the U.S. Army Engineer Research and Development Center (ERDC), has developed a robust multi-dimensional mass conservative finite element hydrodynamic and constituent transport numerical code, Adaptive Hydraulics (ADH). Adaptive Hydraulics has been referred to as "ADH" and "AdH" in literature; the authors utilize the abbreviation "ADH" in accordance with how Adaptive Hydraulics is referenced in peer-reviewed literature.

ADH is a modular code with the capability to simulate varied physics such as saturated and unsaturated groundwater flow, Navier-Stokes flow, and overland flow as well as two-dimensional (2D) shallow water flow. As part of the natural progression of ADH, a three-dimensional (3D) shallow water module (ADH-SW3) has been developed and is currently undergoing testing for robustness, accuracy, and sufficiency of model numerics.

ADH-SW3 represents a generational improvement in USACE's capability to model riverine, estuarine, and reservoir physics because of the following:

1. Linear triangle-based meshing allows for accurate and adequate representation of bathymetry.
2. Vertical meshing that is neither Sigma nor Z-grid based is not encumbered by the drawbacks of either.
3. Run-time adaption in the horizontal and vertical allows for accurate representation of hydrodynamics as well as transport.
4. Internal time-step size adaption allows for time-step changes to capture rapidly changing physics during run time.
5. Fluid and constituent mass are conserved.
6. Easy transition from the (2D) realm to the (3D) realm is accomplished.

Purpose of study

The objectives of this study were to evaluate the capability of ADH-SW3 to accurately replicate hydrodynamics and transport through application to a suite of analytic and experimental flume studies.

Verification and validation approach

The approach utilized in this study was designed to replicate the order in which the code was created. The tests performed in order were as follows:

- Verification tests

  These are tests which are performed to ascertain whether the code is solving the correct equations accurately and involves the solving of analytic problems with known solutions. A verification test is successfully completed if the numerical model can reproduce the analytic solution without any modification to the model parameters from those specified in the analytic problem.

  ADH-SW3 was subjected to the following verification tests:

  - basic tests to ensure that the code is conserving fluid and constituent mass
  - model response to periodic forcing
  - model response to a free-surface seiche in a closed, frictionless basin
  - model response to Coriolis forcing
  - model response to wind forcing
  - model response to combined wind and Coriolis forcing: generation of the Ekman velocity profile.

- Validation tests

  These are tests performed to exercise the code through application to flume studies and/or real world problems. A validation test involves application of the code to the problem where physical parameters such as roughness are known. Modification of model parameters is usually allowed within scientifically acceptable ranges. If observed parameter values are known for the problem, no modification of parameters is allowed.

  A validation test is successfully completed if the numerical model can reproduce the observed results within some scientifically acceptable error range, usually within a 5% range.

  ADH-SW3 was subjected to the following validation tests:

- flow around a spur dike: test of the turbulence closure models
- flow around a submerged trapezoidal spur dike: test of turbulence closure models
- propagation of salinity generated density currents subsequent to a lock exchange
- propagation of temperature-generated density currents within an idealized reservoir.

Mesh convergence and adaption

A basic tenet of numerical modeling is that as the mesh and time-step are refined, a model should converge to the underlying equations that are being solved. In comparisons to the solutions, either analytic or experimental, three different meshes are run:

1. The first mesh is the *base* mesh generated to adequately represent the problem domain.
2. The second mesh has twice the resolution of the base mesh in the horizontal and the vertical. The second mesh is considered to be a high-resolution mesh, and the results are assumed to be converged.
3. ADH-SW3 is an adaptive mesh model, so the mesh resolution is increased automatically (and in some cases removed, but the resolution never goes below the base resolution). This capability allows the model to add resolution when and where needed based on user-supplied parameters. This capability was utilized and considered as the third mesh with the base mesh serving as the initial mesh with increased mesh resolution being added as appropriate through adaption.

Within this verification and validation exercise, it will be demonstrated that adaption is working to give results that are converged with a lesser computational effort. This computational effort roughly correlates with the number of nodes in the mesh.

To prevent an undue increase in the size of this report, the time-step is considered to be converged through the utilization of time-step size adaption. It has been shown (Savant et al. 2011) that the time-step adaption formulation in ADH provides converged results.

Reproducibility

Sound scientific and engineering practice requires reproducibility of test results within reasonable variation (due to code changes, etc.). Provided are the basic model parameters that have an impact on simulation results; these parameters are provided within a table for most of the test cases and include at a minimum the background eddy viscosities, turbulence parameters, and roughness properties.

Number of processor selection

The complexity and scale of problems simulated varied among test cases; this variation necessitated the utilization of a different number of processors for different problems. The number of processors used for each test was decided upon based on the availability of computing resources as well as the scale and complexity of the test being performed. As shown in this document, the number of processors used has an insignificant impact on the computational results and accuracy achieved.

2 Testing

Verification tests

Mass conservation

Mass conservation is a basic tenet of numerical modeling. Numerical codes utilizing the conservative form of the shallow water equations must conserve fluid as well as constituent mass. SW3-ADH is written to be mass conservative, and hence the first test performed on the code was a mass conservation test.

The domain for this test consisted of a cuboid flume 40,000 meters (m) (length) × 8,000 m (width) × 12 m (depth). This domain is represented in Figure 1. The water surface was initially perturbed by 0.25 m at the left-hand wall of the flume and displaced at the right-hand wall by –0.25 m (Figure 2).

This configuration provides an initial volume of fluid in the basin of 3.84 billion cubic meters (m^3). The model is allowed to slosh for 1 day and the fluid volume recalculated. In the absence of external inflows and coding errors, a conservative model must have the same volume of fluid at 86,400 seconds (sec) as was present at 0.0 sec.

Figure 1. Domain for mass conservation test case.

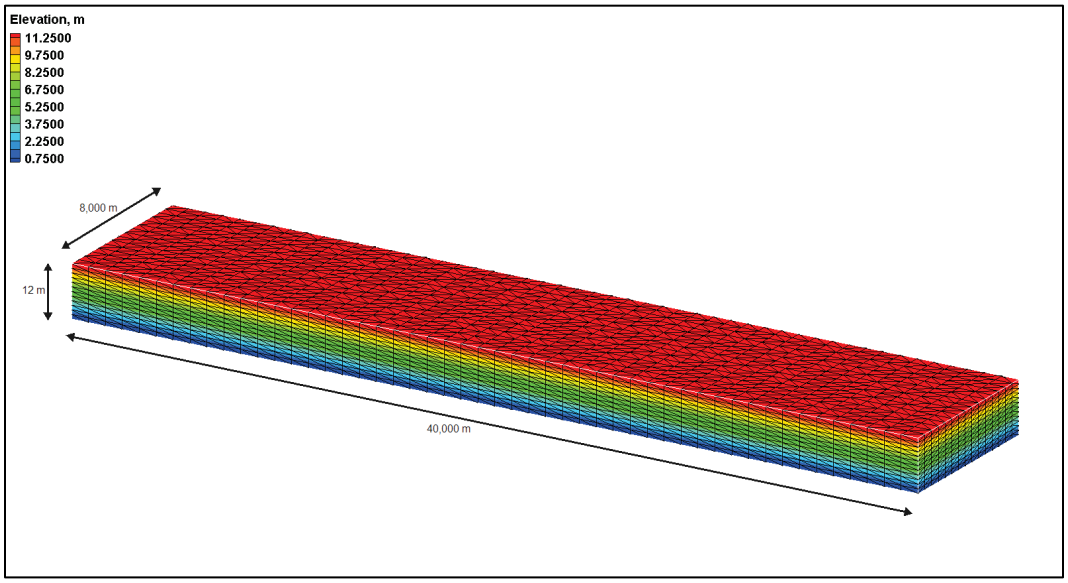

Figure 2. Initial displacement.

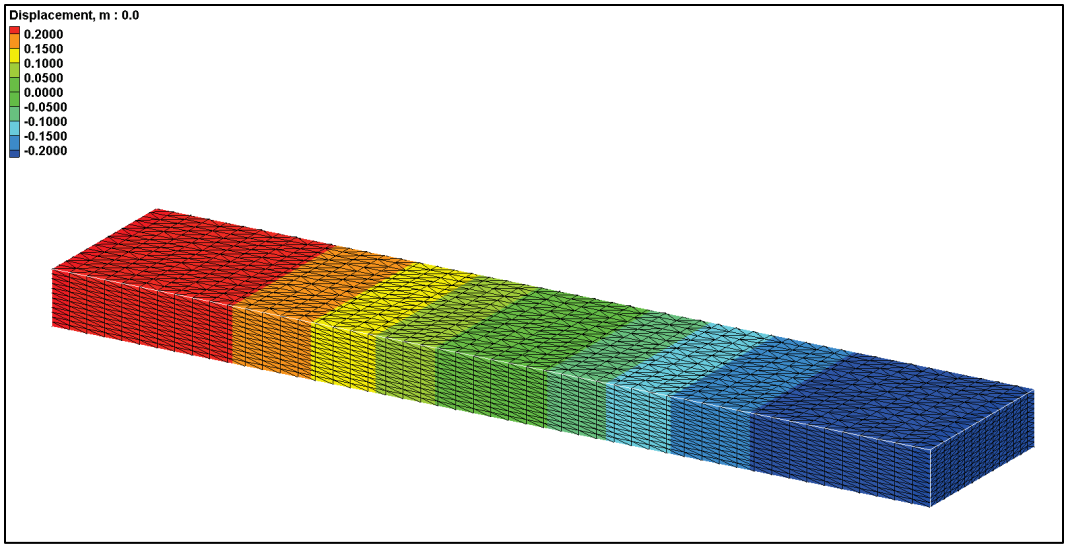

Figure 3 illustrates the final model state (in terms of displacement) at 86,400 sec. As would be expected for a conservative model, the displacement is at 0.0 m (~ 0.0000001 m). This provides a fluid volume of 3.84 billion m^3, the same as the fluid volume at 0.0 sec.

Figure 3. Final displacement.

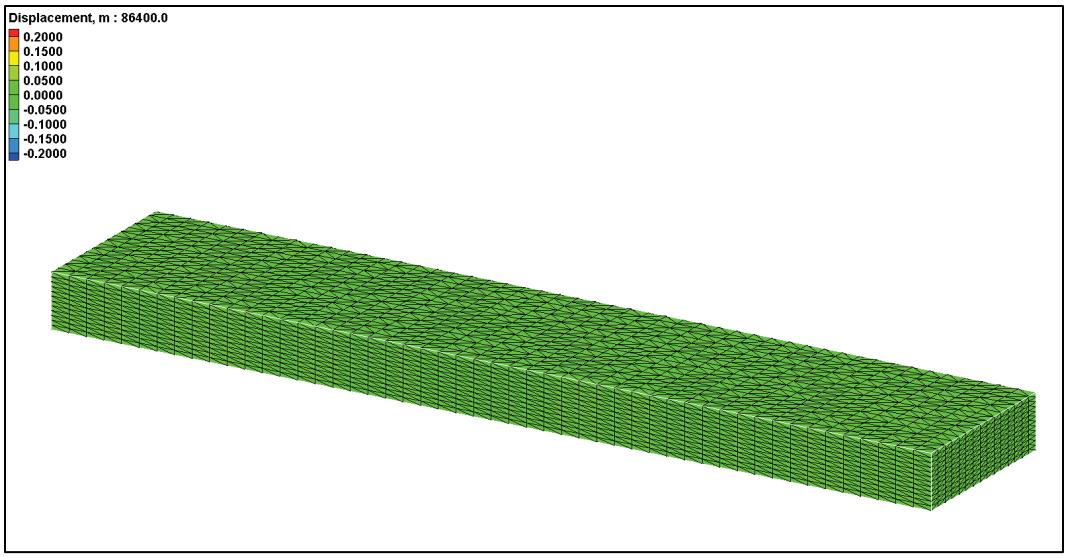

To test constituent mass conservation, the concentration of a generic constituent was specified as 0.035 kilograms/cubic meter (kg/m^3) for a total constituent mass of 134.4 million kg. At the end of simulation, the total mass was conserved, though there were local variations in the exact value of constituent concentrations. These deviations were in general less than 0.002 kg/m^3. Tables 1 and 2 present the results of the mesh resolution test

performed to ascertain the effects of resolution on fluid and constituent mass conservation and the effect of number of processors used, respectively. As expected, the higher resolution mesh provides a slight improvement in the results, and the code provides essentially the same results for both one and six processors. It must be emphasized that both mesh resolutions conserve fluid and constituent mass to at least the non-linear tolerance specified in the ADH-SW3 boundary conditions file.

Table 1. Model behavior for mass conservation tests; number of compute nodes: 1.

Horizontal Node Spacing (m)	Number of Vertical Layers	Total/Max Number of Nodes	Model Water Level (m)	Theoretical Water Level (m)	Water Level Error (m)	Model Concentration (kg/m³)	Theoretical Concentration (kg/m³)	Concentration Error (kg/m³)
800 × 533.33	12	10,608	–4.3391e-009	0.0000	–4.3391e-009	0.034998	0.035	-2.0×10^{-6}
400 × 266.67	24	78,275	–3.6106e-009	0.0000	–3.6106e-009	0.034999	0.035	-1.0×10^{-6}
800 × 533.33, adaption	12, adaption	29,358	–3.5426e-009	0.0000	–3.5426e-009	0.034999	0.035	-1.0×10^{-6}

Table 2. Model behavior for mass conservation tests; number of compute nodes: 6.

Horizontal Node Spacing (m)	Number of Vertical Layers	Total/Max Number of Nodes	Model Water Level (m)	Theoretical Water Level (m)	Water Level Error (m)	Model Concentration (kg/m3)	Theoretical Concentration (kg/m3)	Concentration Error (kg/m3)
800 × 533.33	12	10,608	–4.3256e-009	0.0000	–4.3256e-009	0.034999	0.035	-1.0×10^{-6}
400 × 266.67	24	78,275	–3.5245e-009	0.0000	–3.5245e-009	0.034999	0.035	-1.0×10^{-6}
800 × 533.33, adaption	12, adaption	29,355	–3.5409 e-009	0.0000	–3.5409e-009	0.034999	0.035	-1.0×10^{-6}

Response of model to tidal propagation (periodic forcing) in a closed basin

This case was designed to test the accuracy of the time integration scheme implemented in the code by representing the propagation of an undamped sine wave in a rectangular channel**.** The basin is open at one end, enclosed on all others, and the *free slip* velocity condition is assumed on the internal walls. The model domain is represented in Figure 4. The sine wave applied at the boundary is written as

$$h = (1.0)Sin(t) \quad (1)$$

Figure 4. Model domain

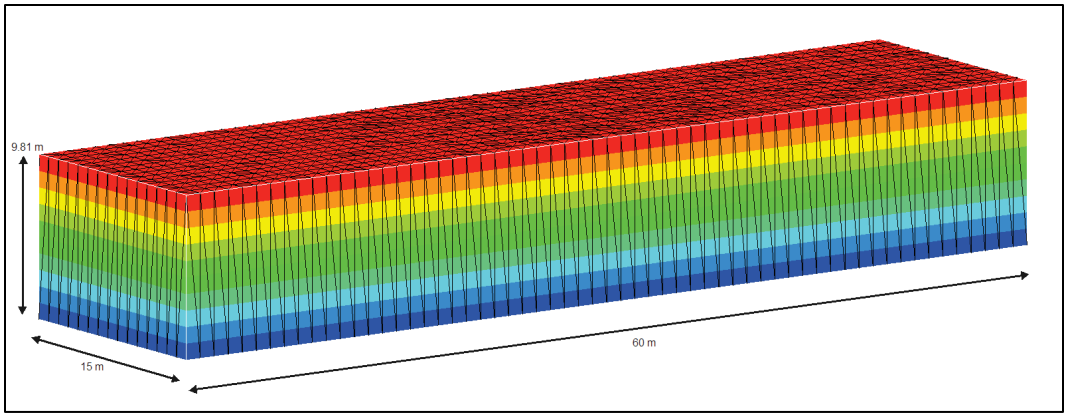

where h is the water surface displacement, and t is the time.

The physical constants are acceleration due to gravity (g = 9.81 meters/second squared (m/s²)) and initial depth (H = 9.81 m).

The analytic spatially and time varying solution of this wave is provided in Taylor and Davis (1975) and is

$$h = (1.0)Sin(t - x / 9.81) \quad (2)$$

where x is the longitudinal distance from the open boundary.

Figure 5 provides a comparison of the analytic solution and the model-generated results. The error between the analytic and the model solution is provided in Figure 6. Tables 3 and 4 provide the test results for 1 and 32 processors, respectively. The results show that the model reproduces the analytic solution with small variations for 1 as well as 32 processors.

Model simulation of free-surface Seiching in a closed rectangular basin

In a frictionless closed basin, the oscillation generated due to an initial perturbation in the free surface is the result of interaction between inertia and gravity. The analytic solution is easily obtained and is represented as

$$\eta = \frac{H}{2}\cos(kx)\cos(\sigma t)$$
$$u = \frac{H}{2}\sigma\frac{\cosh(k(h+z))}{\sinh(kh)}\sin(kx)\sin(\sigma t) \quad (3)$$
$$w = -\frac{H}{2}\sigma\frac{\sinh(k(h+z))}{\sinh(kh)}\cos(kx)\sin(\sigma t)$$

where:

η=water surface elevation
σ = frequency of the wave
u = horizontal x-direction velocity
w = vertical velocity
h = average fluid depth
z = vertical ordinate
H = peak-to-peak wave amplitude
x = horizontal distance
t = time since initialization of the perturbation
k =wave number.

Figure 5. Analytic vs. model-generated results at x = 30 m, y = 15 m.

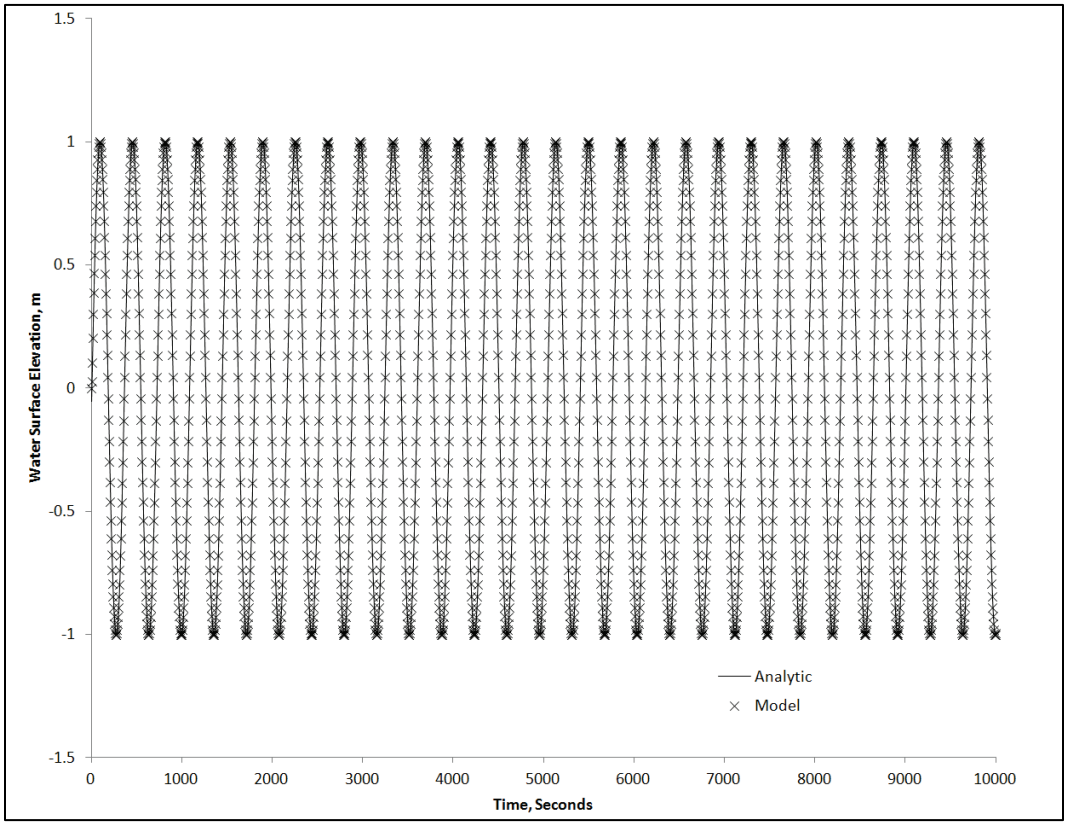

Figure 6. Error between analytic and model-generated results at x = 30 m, y = 15 m.

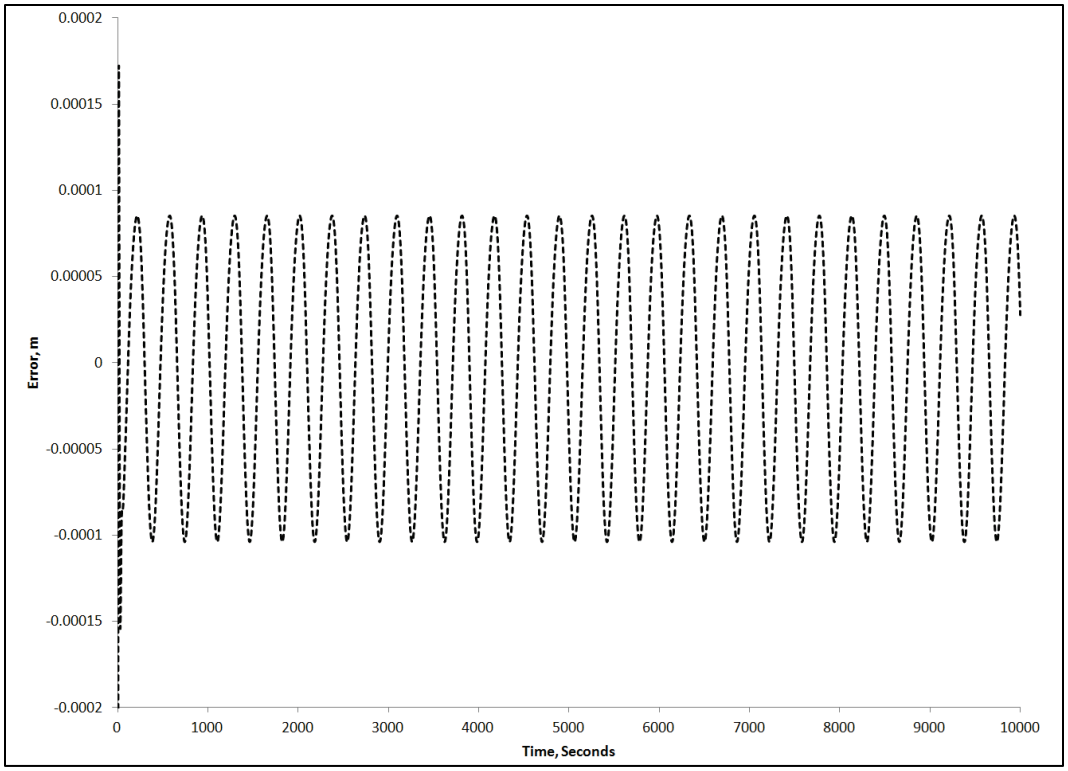

Table 3. Model behavior for periodic forcing tests; number of compute nodes: 1.

Horizontal Node Spacing (m)	Number of Vertical Layers	Total/Max Number of Nodes	Average Water Level Error (m)
1 × 1	1	1,952	–2.6117E-04
0.5 × 0.5	2	11,253	2.5E-04
0.5 × 0.5	12	48,763	2.8005E-04
1 × 1, adaption	1, adaption	2,753	–2.5461E-04

Table 4. Model behavior for periodic forcing tests; number of compute nodes: 32.

Horizontal Node Spacing (m)	Number of Vertical Layers	Total/Max Number of Nodes	Average Water Level Error (m)
1 × 1	1	1,952	–5.24E-04
0.5 × 0.5	2	11,253	3.2148-04
0.5 × 0.5	12	48,763	1.7513-04
1 × 1, adaption	1, adaption	3,259	–4.175-04

The y-direction velocity for a free-surface Seiche in a frictionless closed rectangular basin is zero at all times for all locations within the domain.

For a mode of m, the length of the domain to generate a standing wave is determined as

$$L = \frac{2l}{m} \tag{4}$$

where:

L = wavelength
l = length of the domain
m = wave mode.

The setup of this problem investigates the accuracy of the temporal acceleration term implementation in the ADH-SW3 code. The basic parameters of this problem are presented in Table 5.

Table 5. Problem parameters.

Peak-to-Peak Amplitude (H)	0.5 m
Mean Water Depth (h)	100 m
Wave Mode (m)	1 and 3
Length of Basin (l)	120,000 m
Wavelength (L)	240,000 m and 80,000 m

Under the parameters presented, the wave characteristics result in a standing wave, and the model should reproduce this behavior. This is a linear problem, and ADH-SW3 solves a system of non-linear equations; therefore, it is expected that the model will deviate from the analytic solution for large perturbations in the water surface as time progresses.

Figure 7 presents the initial domain state for the problem with mode m = 3 (red represents 0.25 m and blue represents –0.25 m).

Model parameters for this test are presented in Table 6. Note that all results presented are from the test case where mesh adaption was turned on.

Figures 8 and 9 present the results from the model simulation (modes m = 1 and m = 3, respectively) with the adapted mesh at a free-surface node in the domain located at x = 81,000 m from the left end of the mesh. Please note that results for mode m = 3 exhibit behavior similar to mode m = 1 for displacement as well as velocities.

Figure 7. Domain and initial state for free-surface Seiche problem.

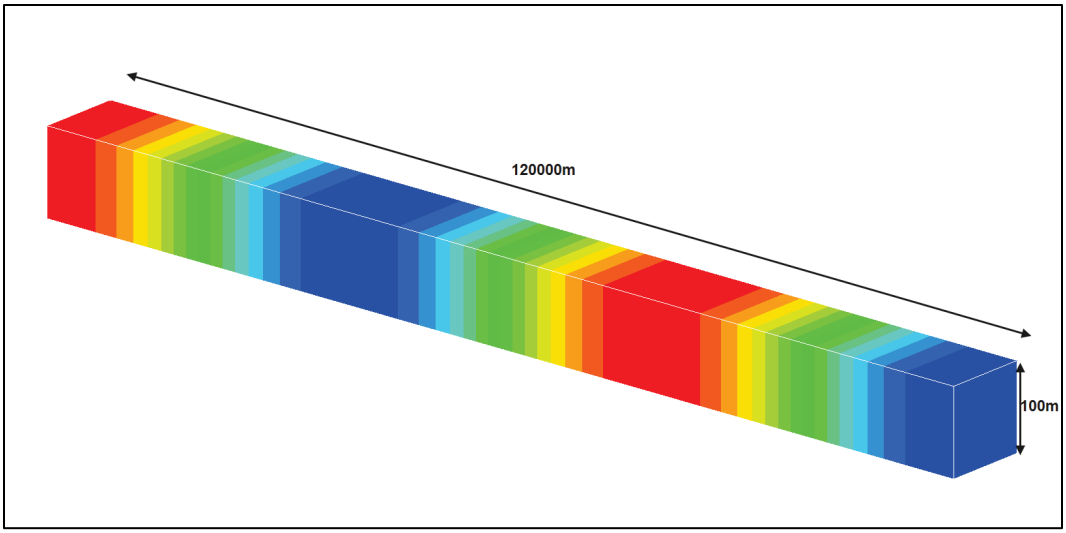

Table 6. Model parameters for free-surface Seiche problem (all modes).

Parameter	Base Mesh	Adapted Mesh	Twice-Refined Mesh
Background Kinematic Eddy Viscosity	0.00	0.00	0.00
Manning's n	0.0	0.0	0.0
Turbulence Model	OFF	OFF	OFF

Figure 8. Displacement results for free-surface Seiche problem; mode $m = 1$.

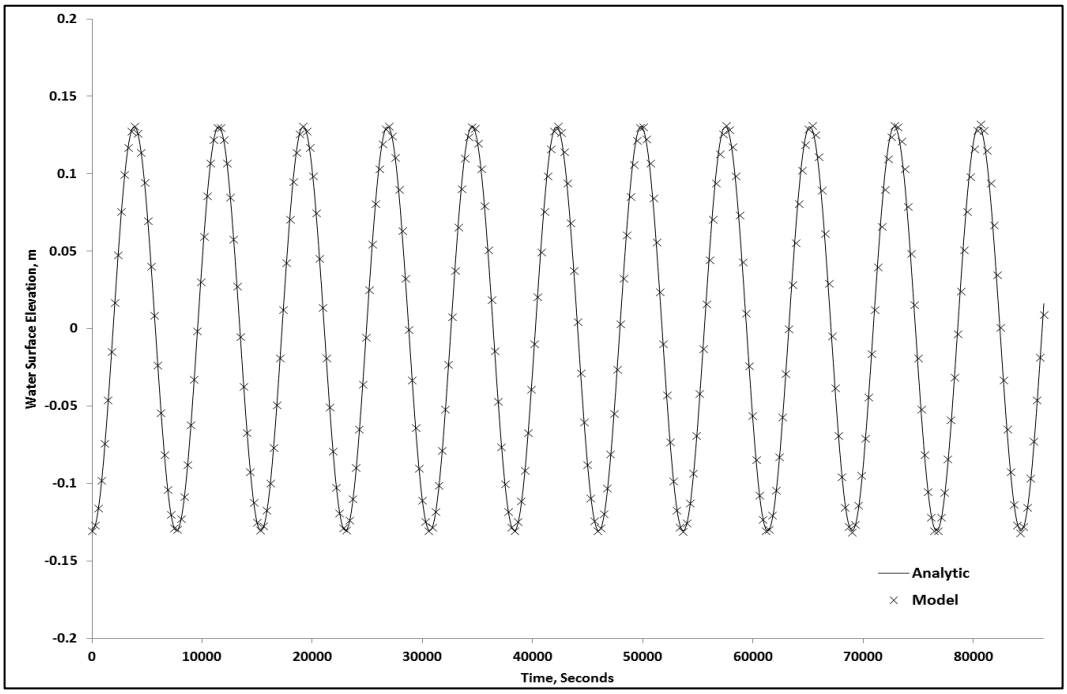

Figure 9. Displacement results for free-surface Seiche problem; mode $m = 3$.

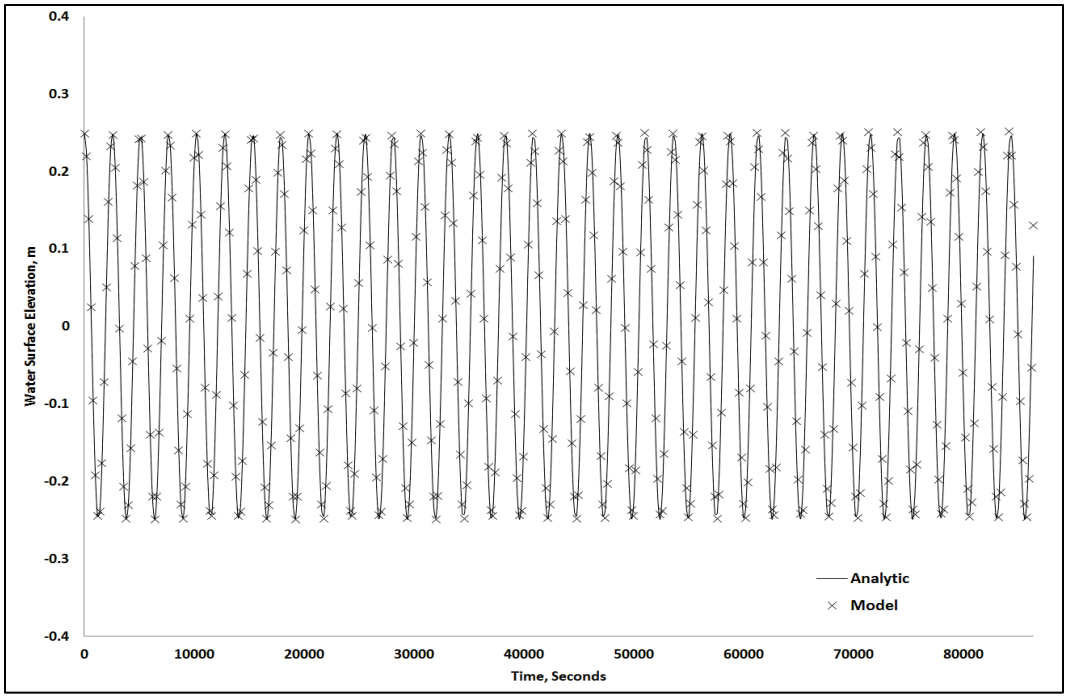

Figures 10 and 11 show the comparisons between the x direction and vertical (z direction) velocities, respectively, for the mode $m = 1$ test case at a free surface node in the domain located at $x = 81{,}000$ m from the left end of the mesh.

Figure 10. x-Direction velocity for free-surface slosh; mode $m = 1$.

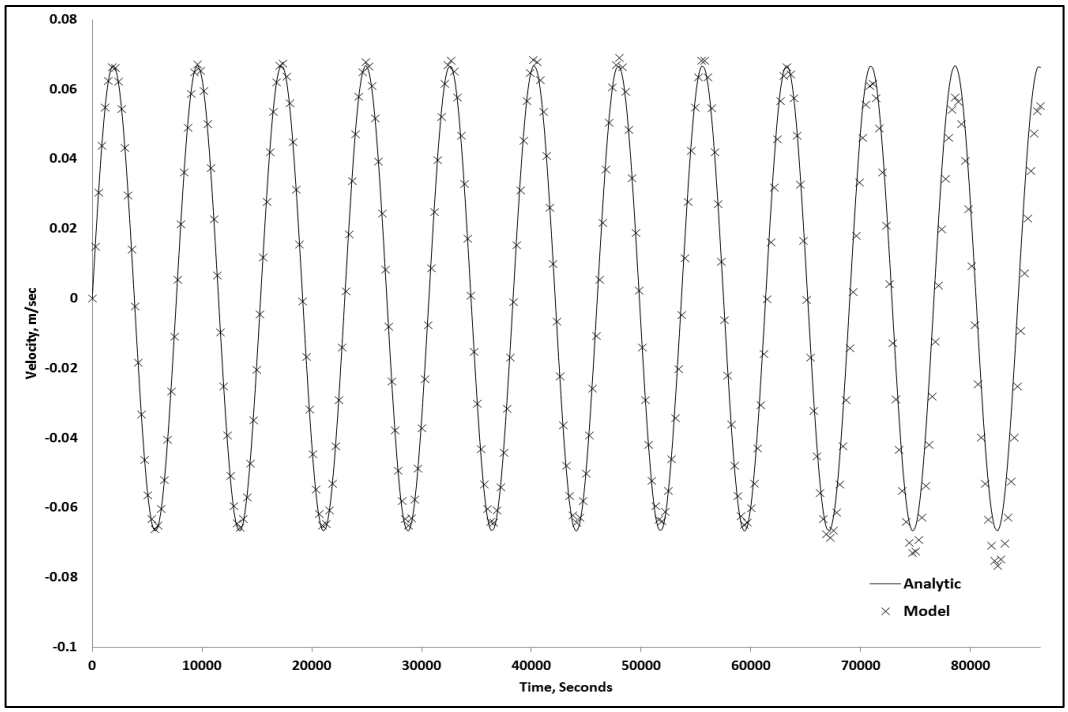

Figure 11. *z*-Direction or vertical velocity for free-surface slosh; mode *m* = 1.

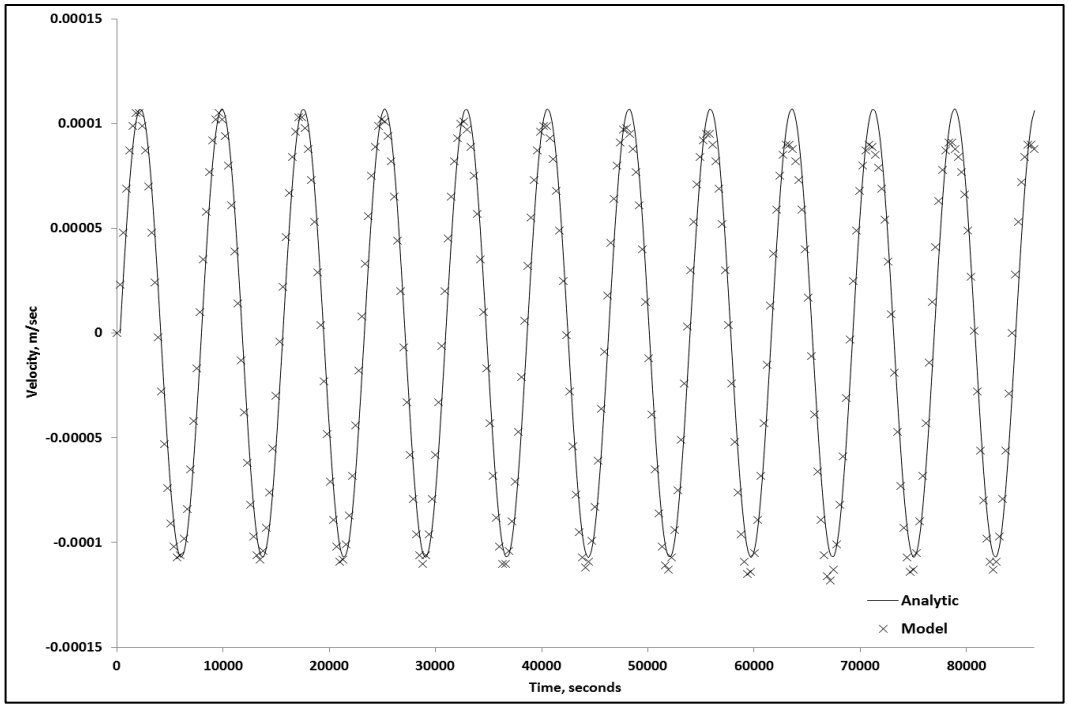

Table 7. Domain discretization and average error; mode m = 1.

Horizontal Node Spacing, *m*	Number of Vertical Layers	Time-step, sec	Average Error (Analytic–Model)		
			Water Surface, m	*X* Velocity, m/sec	*W* Velocity, m/sec
6,000 × 6,000	1	50	–0.00014	0.003	2E-6
3,000 × 3,000	2	50	–0.00001	0.002	1.2E-6
6,000 × 6,000, adaption	1, adaption	50	–0.00003	0.002	1.4E-6

Close examination of Figures 10 and 11 shows that the model computed velocity results diverge from the analytic solution as time progresses. This is an artifact of the right-angle, solid-wall corners that comprise the domain. This is a common issue encountered in handling solid, right-angle corners; the results presented in Wang et al. (2009) show a similar behavior with time. The developers are actively attempting to develop a solution for this corner issue. It must be noted that the vast majority of problems where ADH-SW3 is likely to be applied will, in all probability, not have sharp 90° corners. If and when these corners are encountered, the solution is relatively easy and involves artificially increasing the eddy viscosity to slightly above background levels and/or rounding the corner.

Model response to Coriolis forcing

A simplified system was set up to test the water surface slope variation in the x direction and the y direction due to Coriolis forcing.

The flume for the x-direction test has a flat bottom and is dimensioned as shown in Figure 12. The x- and y-direction momentum equations are written as

$$\rho\left(\frac{\partial u}{\partial t}+u\frac{\partial u}{\partial x}+v\frac{\partial u}{\partial y}+w\frac{\partial u}{\partial z}\right)-\nabla\sigma_x+\frac{\partial P}{\partial x}-(2\omega sin\theta)v=0 \quad \text{x-direction} \tag{5}$$

$$\rho\left(\frac{\partial v}{\partial t}+u\frac{\partial v}{\partial x}+v\frac{\partial v}{\partial y}+w\frac{\partial v}{\partial z}\right)-\nabla\sigma_y+\frac{\partial P}{\partial y}-(2\omega sin\theta)u=0 \quad \text{y-direction} \tag{6}$$

where:

u, v and w = x-, y- and z-direction velocities, respectively
ρ = fluid density
P = hydrostatic pressure
σ_x and σ_y = x- and y-direction shear stress, respectively
ω = angular velocity of the earth
θ = latitude.

Figure 12. Test domain for x-direction Coriolis forcing test. The x-axis is along the long axis, the y-axis is along the width (5,000 m), and z-axis is along the depth (1 m). Colors indicate depth with red representing zero depth at the free-surface and blue representing the greatest depth at the bed.

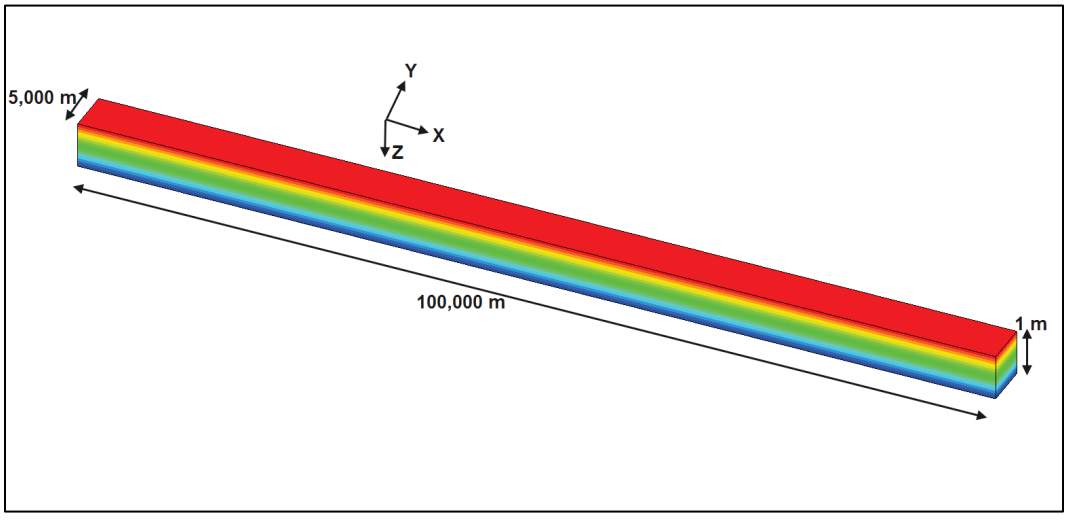

Under frictionless conditions, σ_x and σ_y reduce to zero. The hydrostatic pressure (P) is represented as

$$P = \rho g h \tag{7}$$

where:

g = acceleration due to gravity
h = water depth.

For steady-state conditions, the y velocity is zero, the change in the u (x-direction) velocity with respect to x is zero for a given y, and the vertical velocity (w) is assumed to be negligible everywhere. Therefore, the x equation simplifies to zero, and the y equation reduces to

$$\frac{\delta h}{\delta y} = -\frac{2\omega \sin\theta u}{g} \tag{8}$$

Using the known parameters and latitude of 45°, the water surface slope should be –2.0988E-6 m/m. The model simulation provides a slope of –2.154E-6 m/m (Figure 13). The velocity direction indicates a curvature toward the right (Figure 14) which is supported by the Coriolis theory.

Figure 13. ater surface elevation variation along the test flume (plan view).

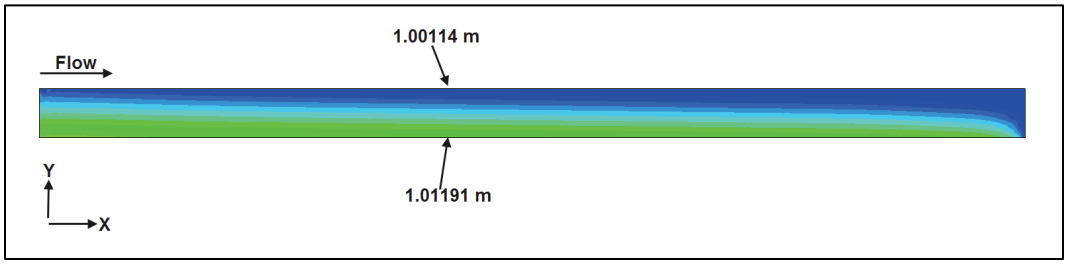

Figure 14. Velocity behavior for the *x*-direction Coriolis test (plan view).

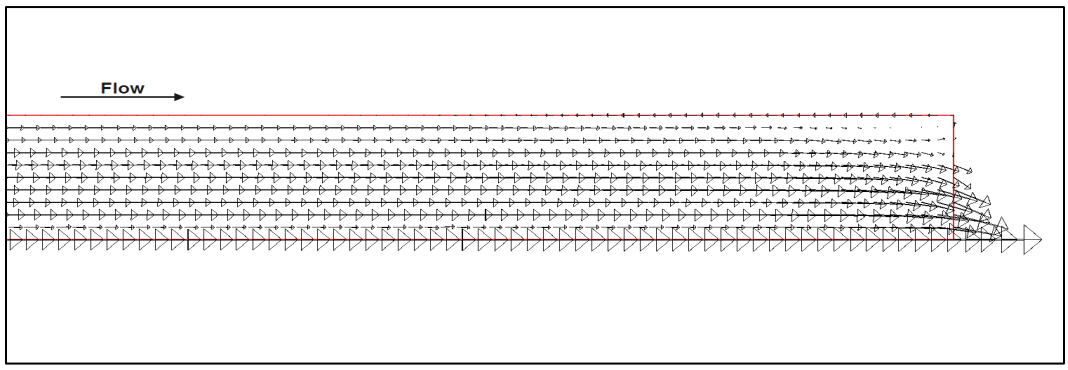

The flume for the *y*-direction test has a flat bottom and is dimensioned as shown in Figure 15 (the image is rotated for ease of illustration). For steady-state conditions, the *x* velocity is zero and the change in the *v* (*y* direction) velocity with respect to *y* is zero for a given *x*. Therefore, the *y* equation simplifies to zero, and the *x* equation reduces to

$$\frac{\delta h}{\delta x} = -\frac{2\omega \sin\theta v}{g} \tag{9}$$

Figure 15. Test domain for *y*-direction Coriolis forcing test.

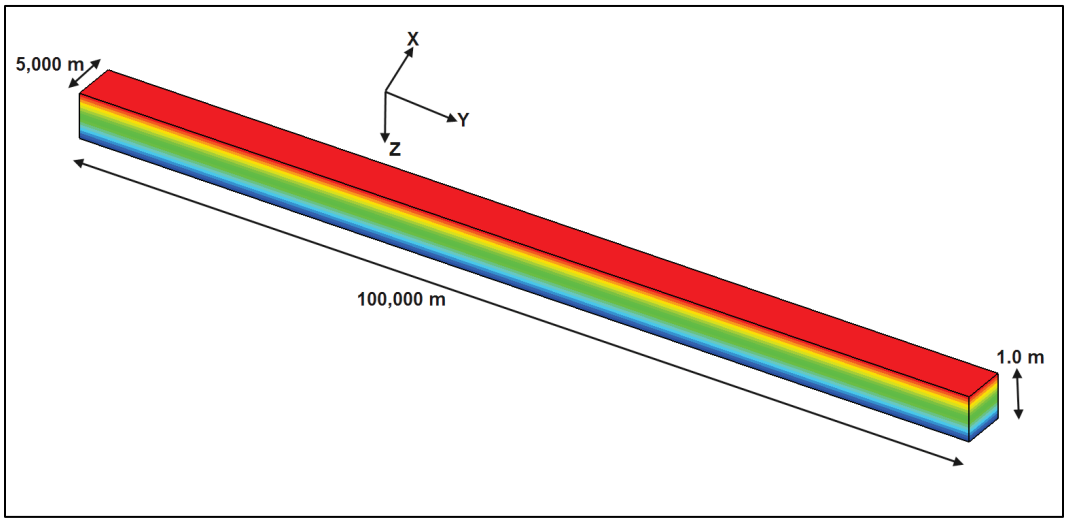

Using the known parameters, the water surface slope, again, should be -2.0988E-6 m/m. The model simulation provides a slope of –2.0000E-6 m/m (Figure 16). The velocity direction (Figure 17) indicates a curvature toward the right which is again supported by the Coriolis theory. Tables 8 and 9 tabulate the results obtained for this case and show that the code is accurately reproducing the analytic solution for Coriolis forcing.

Figure 16. Elevation variation along the test flume.

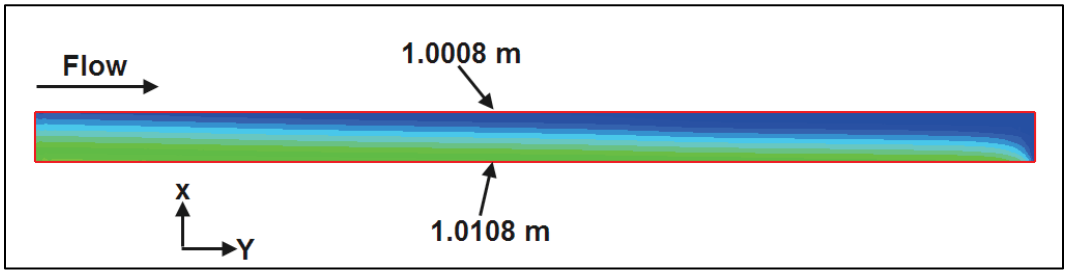

Figure 17. Velocity behavior for the *y*-direction Coriolis test.

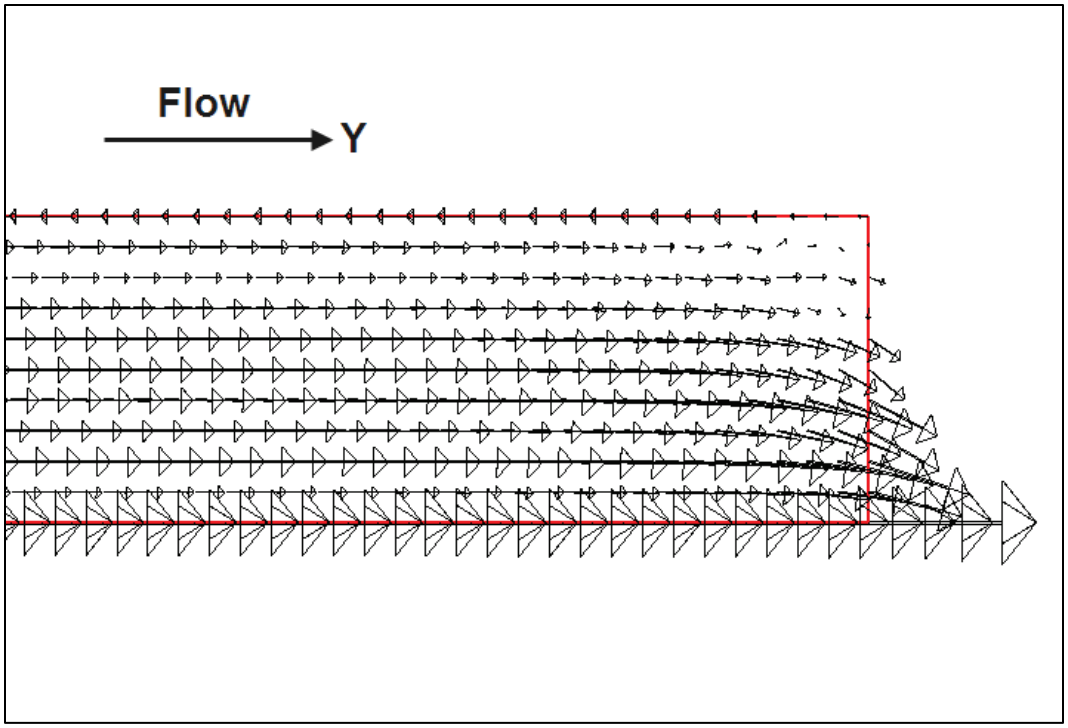

Table 8. Simulation results for *x*-direction Coriolis test case; number of compute nodes: 96.

Horizontal Node Spacing (m)	Number of Vertical Layers	Total/Max Number of Nodes	Slope (m/m)	Analytic Slope (m/m)	Slope Error
500 × 500	5	13,266	–2.154e-6	–2.0988e-6	5.58e-8
250 × 250	8	92,631	–2.118e-6	–2.0988e-6	1.92e-8
500 × 500, adaption	5, adaption	15,894	–2.121e-6	–2.0988e-6	2.22e-8

Table 9. Simulation results for *y*-direction Coriolis test case; number of compute nodes: 96.

Horizontal Node Spacing (m)	Number of Vertical Layers	Total/Max Number of Nodes	Slope (m/m)	Analytic Slope (m/m)	Slope Error
500 × 500	5	13,266	–2.000e-6	–2.0988e-6	9.88e-8
250 × 250	8	92,631	–2.058e-6	–2.0988e-6	4.08e-8
500 × 500, adaption	5, adaption	15,895	–2.025e-6	–2.0988e-6	7.38e-8

Model response to wind forcing

A simplified system was set up to test the water surface slope and 3D return current generated by applying a constant wind shear to the water surface. The flume shown in Figure 18 had a flat bottom with an initial

spatially constant 40 m water depth. The test simulations had the flume oriented in three different directions (the x direction, y direction, and at a 45° angle to the x direction) to properly test the wind application in both the x and y directions independently and then concurrently for the 45° configuration. All wind shears were applied such that the shear direction was oriented in the same direction as the flume.

Figure 18. Test domain for wind-shear test cases.

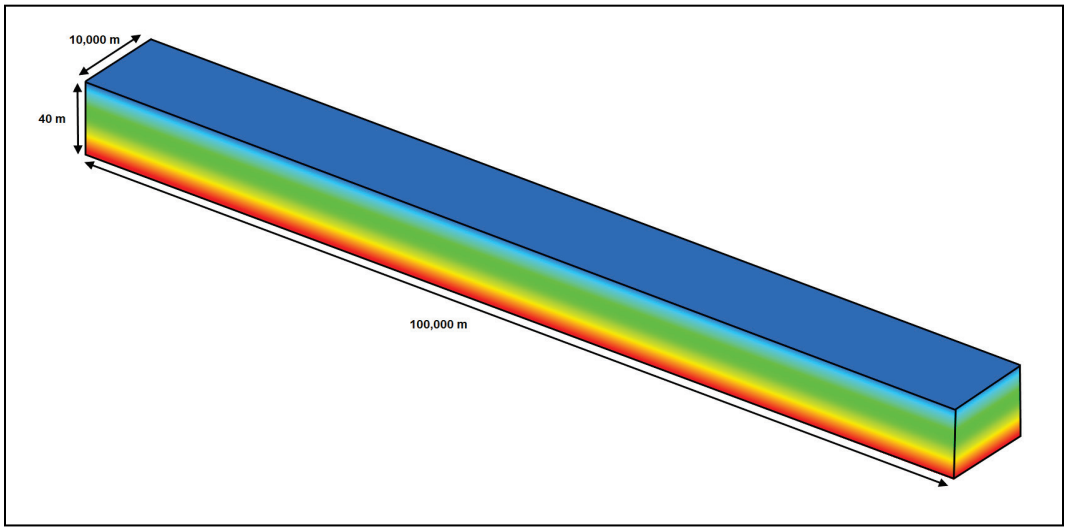

The simulations also investigated the relative error associated with changes in the magnitude of the wind shears (simulated wind shears of 0.1 Newtons per square meter (N/m²) and 0.5 N/m²) along with the impact of varying both the horizontal resolution (500 m and 1,000 m) and vertical mesh resolutions (6, 8, 12, and 20 vertical layers).

The analytical water surface elevation was calculated using

$$\Delta h = \frac{\tau L}{\rho g h} \tag{10}$$

where:

τ = applied wind shear ($\tau = 0.1\ \frac{N}{m^2}$ and $\tau = 0.5\ \frac{N}{m^2}$)
L = length of the flume ($L = 100{,}000\ m$)
ρ = density of water ($\rho = 1{,}000\ \frac{kg}{m^3}$)
g = gravity ($g = 9.817\ \frac{m}{s^2}$)
h = flume depth ($h = 40\ m$)

Δh = change in water level along the length of the flume (Wang et al. 2009).

The analytical solution for the vertical velocity profile for an infinitely long flume at any point along the x direction is

$$u = \frac{1}{6K_v} gSh^2 \left[3(\delta - 1)^2 - 1\right] + \frac{\tau h}{2\rho K_v}(2\delta - 1) \quad (11)$$

where:

K_v = constant vertical eddy viscosity ($K_v = 0.03 \frac{m^2}{s}$)
S = water level slope
δ = non-dimensional or normalized vertical coordinate measure from the bed ($\delta = 0$) to the water surface ($\delta = 1$)
u = velocity for the specified depth (Wang et al. 2009).

The ADH-SW3 water surface elevation solutions for all three flume orientations are shown in Figure 19 for the $\tau = 0.1 \frac{N}{m^2}$ wind shear.

Figure 19. Depths for the three flume orientations with a constant wind shear of 0.1 N/m².

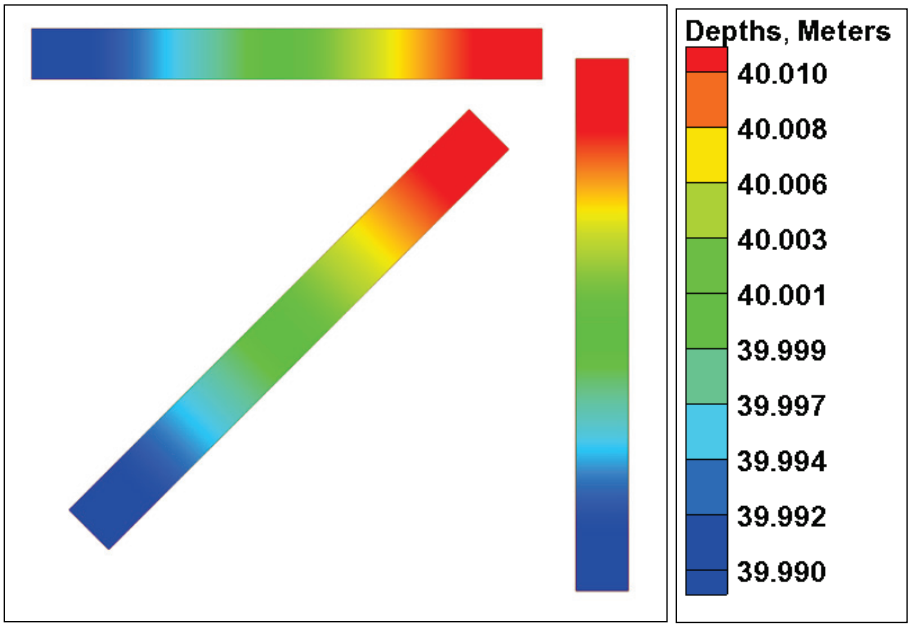

Figures 20 and 21 provide the ADH-SW3 velocity solution for the x-direction-oriented flume for wind shears of 0.1 $\frac{N}{m^2}$ and 0.5 $\frac{N}{m^2}$.

Figure 20. Velocity comparisons with a constant wind shear of 0.1 N/m².

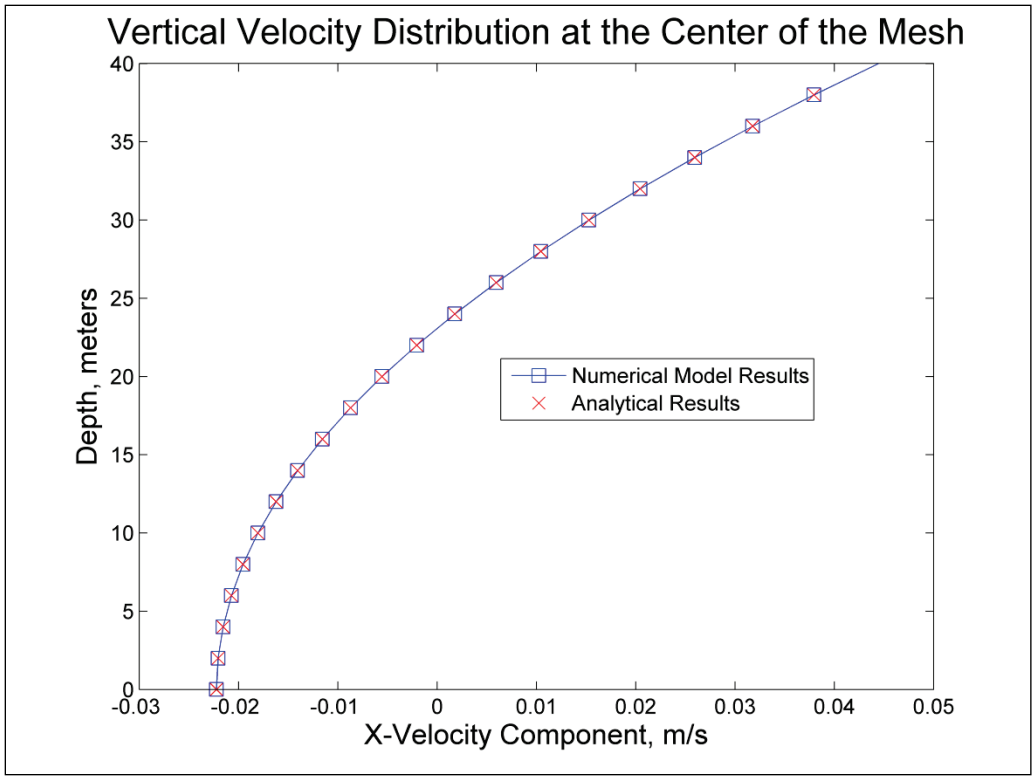

Figure 21. Velocity comparisons with a constant wind shear of 0.5 N/m².

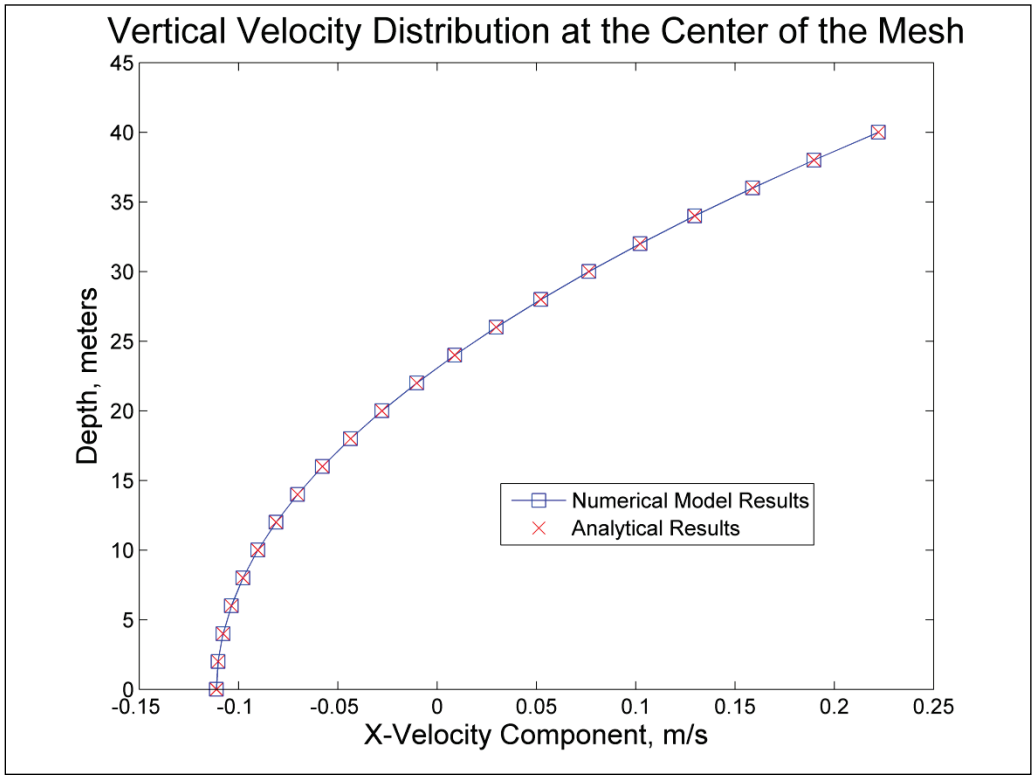

Table 10 provides comparisons of the model results to the analytical head differences along the flume and velocity values for all simulated configurations.

Table 10. Comparison of the ADH-SW3 model results to the analytical solution for all simulated scenarios.

Horizontal Node Spacing (m)	Number of Vertical Layers	Wind Shear Applied (N/m2)	Flume Orientation	Velocity - Root Mean Square Error (m/s)	Model Water Level Difference Over Flume Length (m)	Analytical Water Level Difference Over Flume Length (m)	Error in Model Water Level Difference (m)
500	20	0.1	*x* Direction	2.0×10^{-6}	0.02545	0.02547	1.4×10^{-5}
500	20	0.1	*y* Direction	2.0×10^{-6}	0.02545	0.02547	1.4×10^{-5}
500	20	0.1	45 ° from *x*-axis	2.0×10^{-6}	0.02545	0.02547	1.4×10^{-5}
500	20	0.5	*x* Direction	3.0×10^{-5}	0.12754	0.12733	2.1×10^{-4}
500	20	0.5	*y* Direction	3.0×10^{-5}	0.12754	0.12733	2.1×10^{-4}
500	20	0.5	45 ° from *x*-axis	3.0×10^{-5}	0.12754	0.12733	2.1×10^{-4}
500	12	0.1	*x* Direction	5.4×10^{-5}	0.02545	0.02547	1.8×10^{-5}
500	8	0.1	*x* Direction	1.7×10^{-4}	0.02544	0.02547	3.0×10^{-5}
500	6	0.1	*x* Direction	2.9×10^{-4}	0.02542	0.02547	4.1×10^{-5}
500	3	0.1	*x* Direction	6.4×10^{-4}	0.02602	0.02547	5.6×10^{-4}
1,000	20	0.1	*x* Direction	4.5×10^{-5}	0.02538	0.02547	8.3×10^{-5}
2,000	20	0.1	*x* Direction	8.2×10^{-4}	0.02537	0.02547	9.3×10^{-5}

Model response to combined wind and Coriolis forcing: generation of the Ekman velocity profile

This test is designed to replicate the Ekman layer. Ekman layer is the fluid layer where the Coriolis force, the force due to pressure gradient, and the turbulent drag are in balance. This is a unique test case as it tests the implementation of all three forces in the code.

The analytic solution for the Ekman velocity profile or the Ekman Spiral was developed by Ekman and is provided in Price et al. (1987) as

$$U = V_0 e^{\left(-z/D\right)} \cos\left(\frac{\pi}{4} - \frac{z}{D}\right) \tag{12}$$

$$V = V_0 e^{\left(-z/D\right)} sin\left(\frac{\pi}{4} - \frac{z}{D}\right) \quad (13)$$

$$V_0 = \frac{\tau}{\rho\left(Af\right)^{0.5}} \quad (14)$$

$$D = \left(2\frac{A}{f}\right)^{0.5} \quad (15)$$

$$f = 2\omega sin\theta \quad (16)$$

where:

U and V = x and y direction velocity components, respectively
V_0 = surface amplitude
τ = wind stress
ρ = fluid density
f = Coriolis parameter
A = eddy viscosity
D = e-folding depth
z = depth taken positive downward
ω = angular velocity of the Earth in radians/sec
θ = latitude.

The mesh developed for this test case is illustrated in Figure 22 and is a cuboid with dimensions of 4000 kilometers (km) (length) × 4000 km (width) × 200 m (depth). To prevent boundary influences on the test, only material 1 was subjected to the Coriolis and Wind forces. The number of vertical layers was specified as 50, providing a depth of 4 m for each vertical layer. Model parameters utilized are provided as follows:

- Smagorinsky coefficient: 0.0
- Vertical Turbulence Model: OFF
- Uniform background eddy viscosity (A): 0.1 m²/sec
- Mannings *n* value: 0.0
- Wind Stress: 0.1 pascal (Pa) in the *x* direction.
- Latitude (θ): 45°

Figure 22. Mesh and material representation for Ekman profile test.

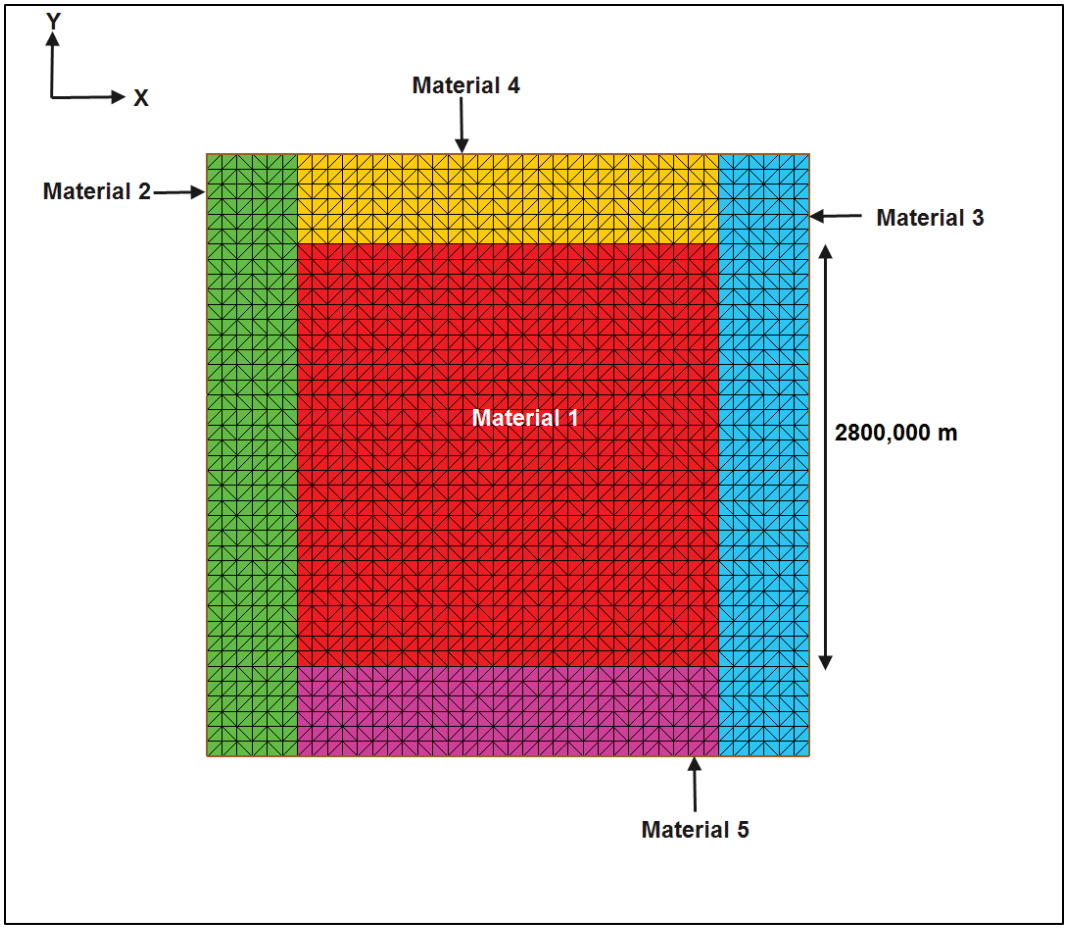

Using these values, the computed values of V_0 and D are 0.0284 rad^{-1} and 40.2 m, respectively.

Figure 23 provides an illustration of the model computed velocities with depth (vector length corresponds to the velocity magnitude) at center of the domain (x = 2000 km, y = 2000 km). Notice that as expected, the velocities rotate as a consequence of the force balance between Coriolis, wind, and turbulent drag.

Figures 24 and 25 show the comparison between the x and the y component of the model-computed velocity with the analytic solution, respectively, and Figure 26 presents the error in the computed velocity magnitude. Note that the model-computed velocities and the analytic velocities differ by an average of ~ 0.0015 m/sec (Table 11). This indicates that the code is indeed computing the pertinent forces and balancing them properly; however, Figures 24 and 25 show a persistent error in the simulation results.

Figure 23. Velocity variation with depth.

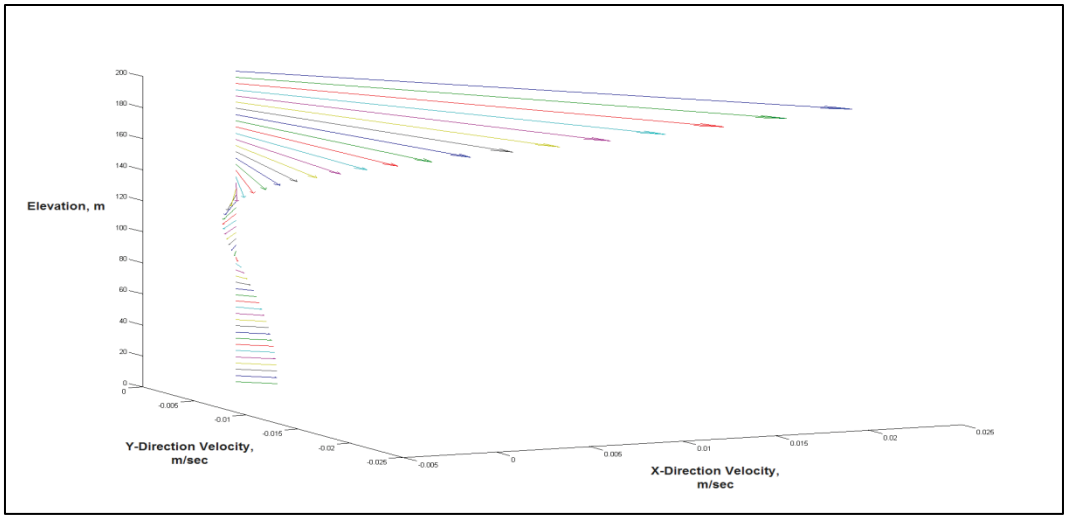

Figure 24. *x*-Direction model and analytic velocities.

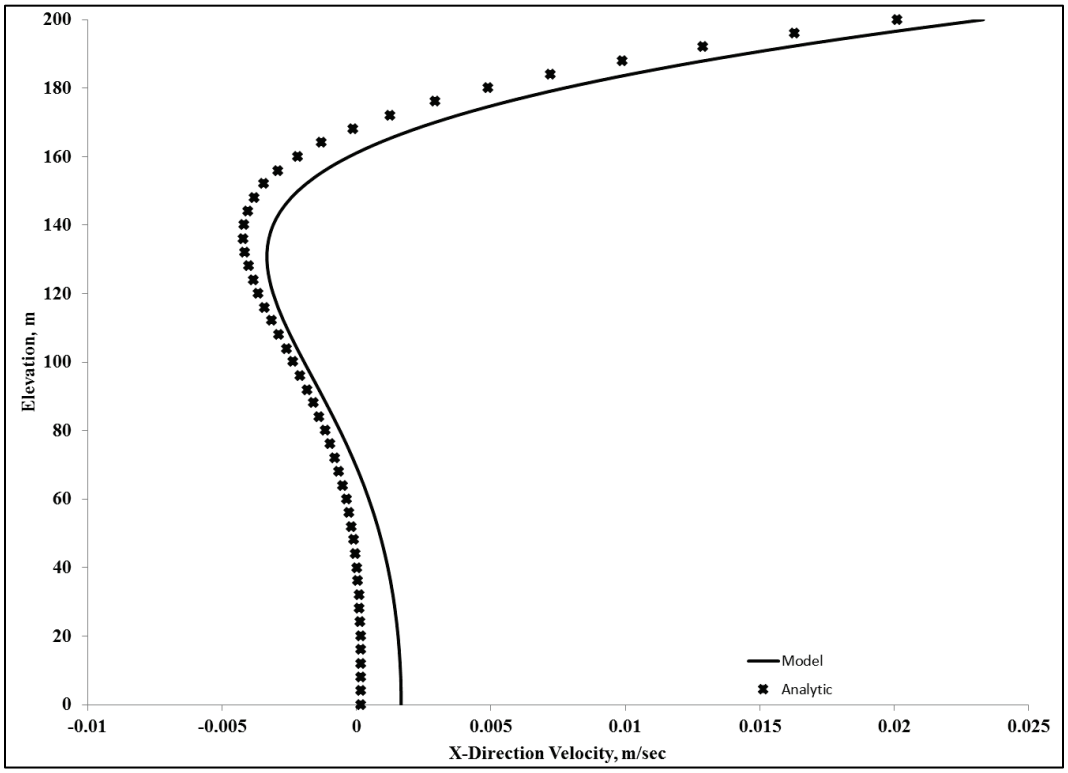

Figure 25. *y*-Direction model and analytic velocities.

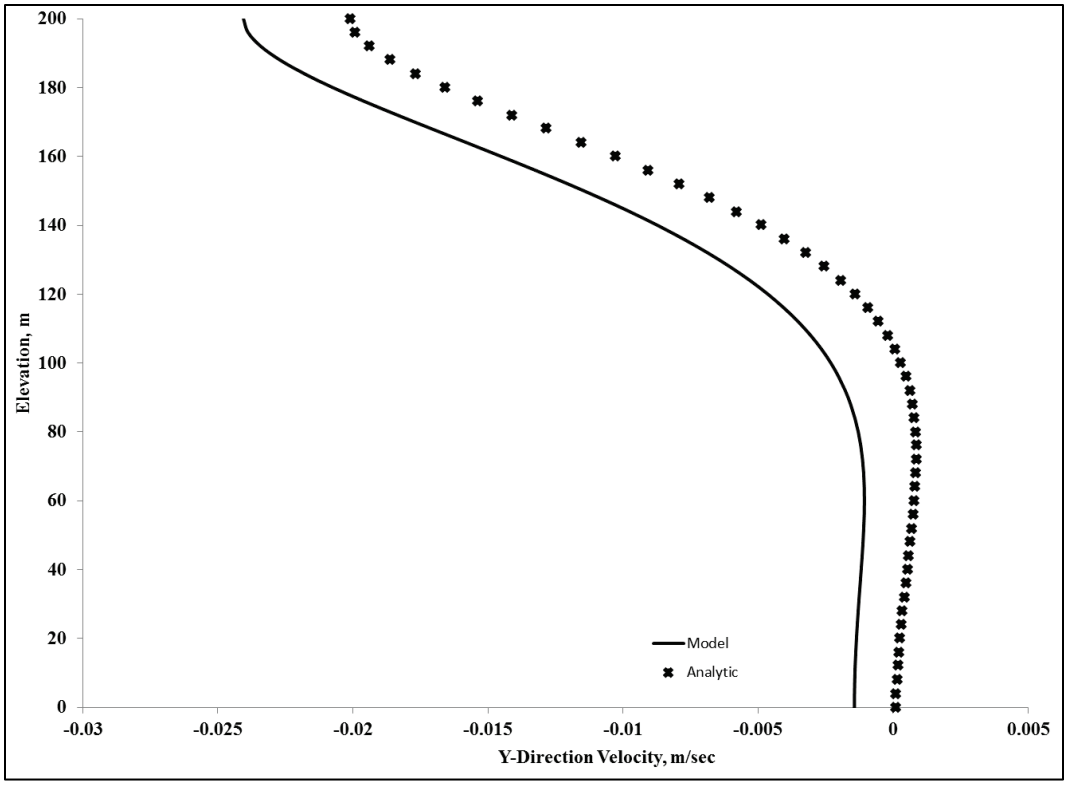

Figure 26. Model and analytic velocities error.

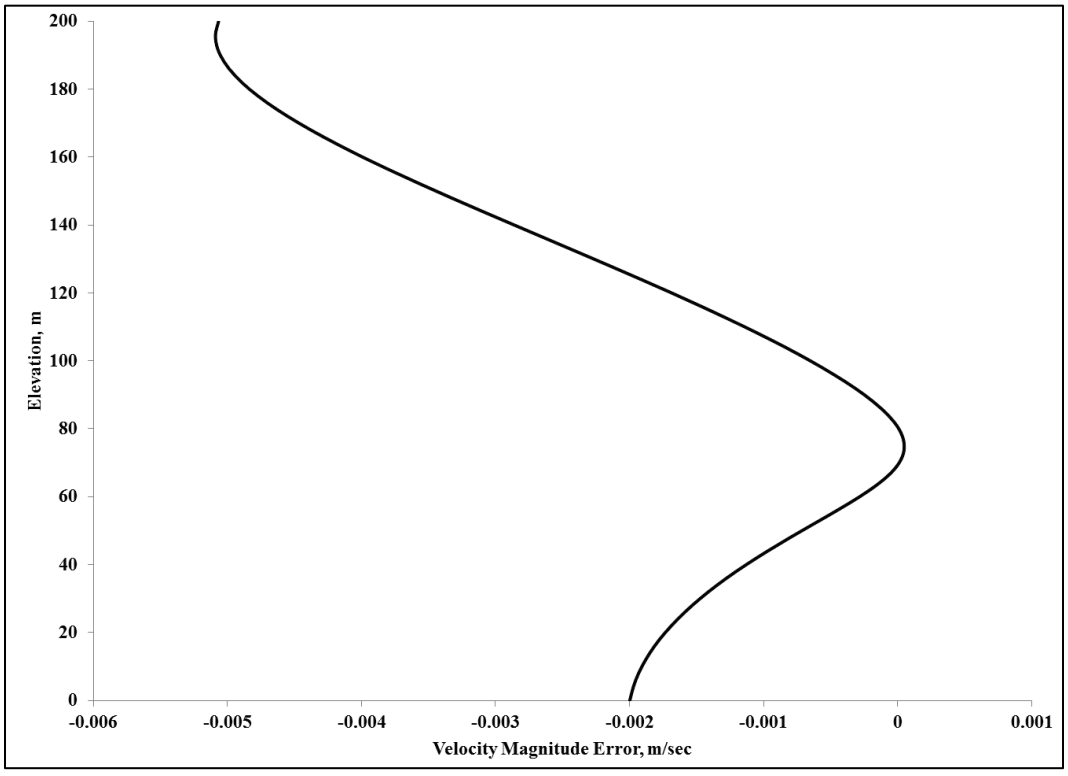

Table 11. Mesh parameters.

Horizontal Node Spacing (m)	Number of Vertical Layers	Total/Max Number of Nodes	Average Velocity Error (m/sec)
100,000 × 100,000	50	85,731	–0.0016
50,000 × 50,000	100	1,292,800	–0.001
100,000 × 100,000 adaption	4, adaption	85,731	–0.0012

The error observed is a result of the boundary effects and indicates that the boundary manipulation performed to mimic an infinite ocean is inadequate. This deduction is corroborated by results from another run with a wind-shear stress of 0.05 Pa instead of the larger 0.1 Pa shear stress. These results are provided in Figure 27, where the velocity is projected onto the *z* plane. Note that the error in the solution is much smaller than the 0.1 Pa simulations, and furthermore, the computed and analytic solutions appear to converge at zero and elsewhere. The authors emphasize that this boundary manipulation is not required for real-world applications as appropriate water level or discharge boundaries will be available through observation data.

Figure 27. Comparative results for 0.1 and 0.05 Pa shear-stress simulations.

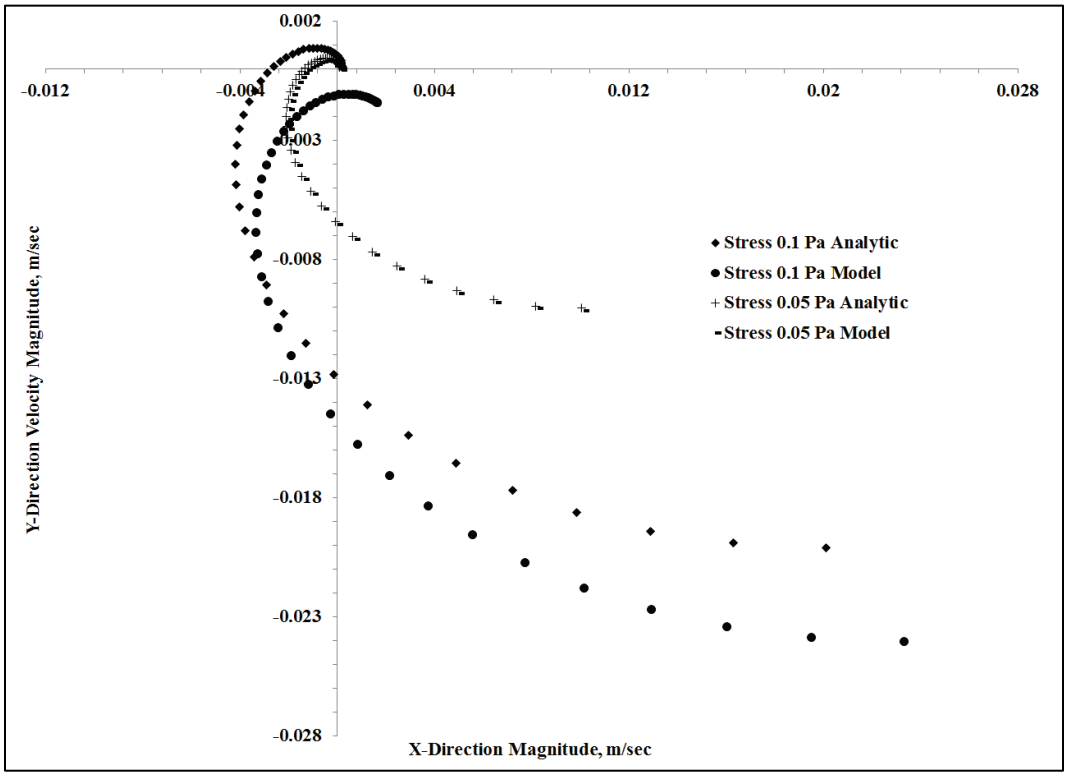

Validation tests

Flow around an emergent spur dike: test of turbulence closure

This test, based upon the work presented in Rajaratnam and Nwachukwu (1983), is designed to test the accuracy and adequacy of the turbulence closure schemes implemented in ADH-SW3. The schemes currently included in the code are the 2nd order Mellor and Yamada (1982) in the vertical and Smagorinsky (1963) in the horizontal.

The test domain is illustrated in Figure 28. An emergent spur of 0.152 m length and 0.03 m width is placed 14.0 m downstream of the inflow location (at the left boundary). A uniform flow of 0.0453 cubic meters per second (m^3/sec) is applied at the left boundary with a tail water elevation of 0.189 m applied at the right boundary.

Figure 28. Plan view of domain for spur-dike test.

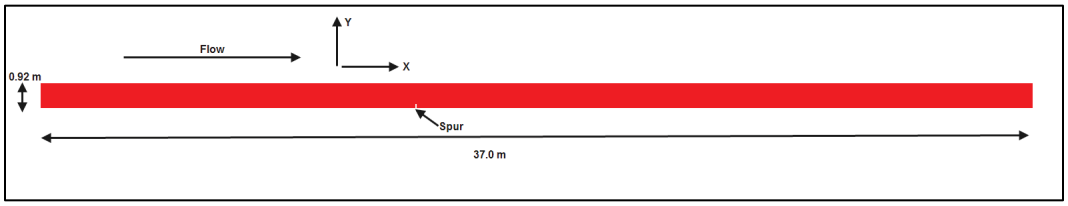

The model parameters utilized are as follows:

- Smagorinsky coefficient: 0.2
- Uniform background eddy viscosity: 0.0015 m^2/sec
- Mannings *n* value: 0.01.

Figure 29 shows the model-computed recirculation at steady flow. The model computed a reattachment length of 11.8 times the spur length.

Figure 29. Model-computed recirculation zone.

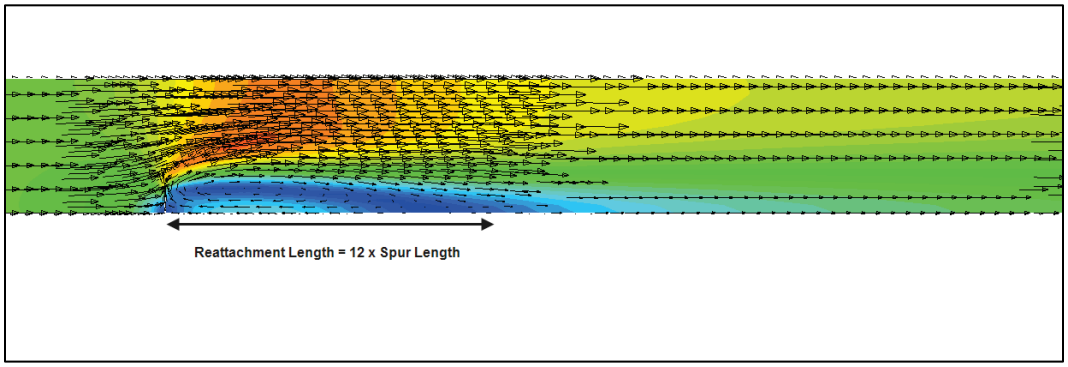

This value matches closely to the value of 12 times the spur length reported in literature (Wang et al. 2009). Figure 30 illustrates the recirculation zone in the *z* or vertical plane. Table 12 lists simulation results for flow around a spur dike test case.

Figure 30. Oblique view of model-computed recirculation zone in the vertical or *z*-axis.

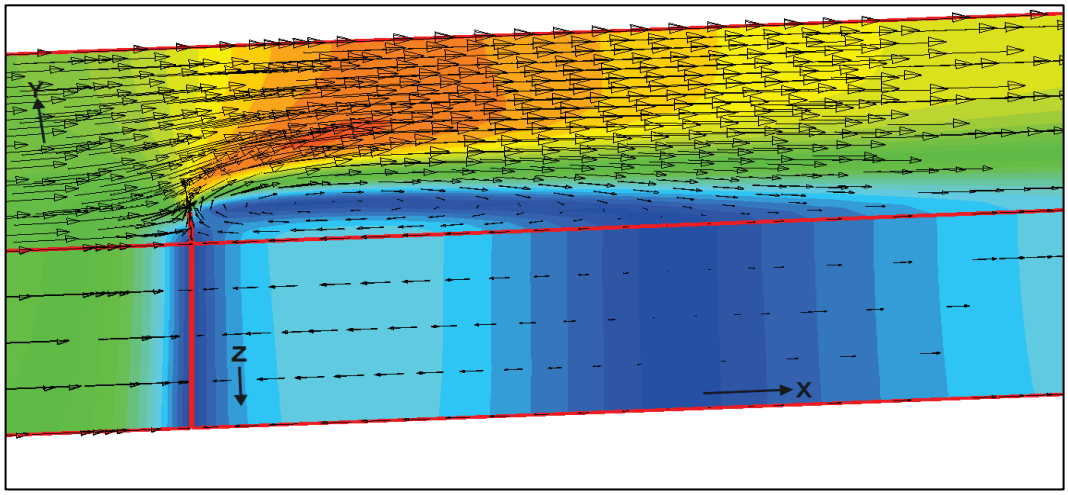

Table 12. Simulation results for flow around a spur dike test case; number of compute nodes: 96.

Horizontal Node Spacing (m)	Number of Vertical Layers	Total/Max Number of Nodes	Re-attachment Length (× Spur Length)
0.1 × 0.1	4	31,500	11.83
0.05 × 0.05	8	219,195	11.95
0.1 × 0.1, adaption	4, adaption	31,734	11.89

Flow around a submerged trapezoidal spur dike: test of turbulence closure

This test, based upon the work presented in Kuhnle et al. (1999) and Wang et al. (2009), is designed to test the accuracy and adequacy of the turbulence closure schemes implemented into the model. The schemes currently implemented in the model are the 2nd order Mellor Yamada (1982) in the vertical and Smagorinsky (1963) in the horizontal.

Figures 31 and 32 show the domain (200 m × 1.2 m × 0.302 m) and the spur dike, respectively. The flow is around and over a submerged trapezoidal dike. The domain of the test problem was extended on the downstream to minimize the effects of downstream boundary on flow near the dike.

Figure 31. Domain.

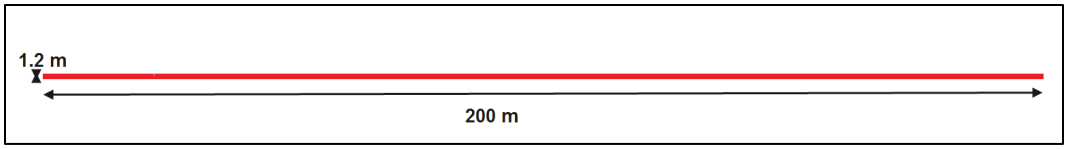

Figure 32. Partial trapezoidal dike in flow field.

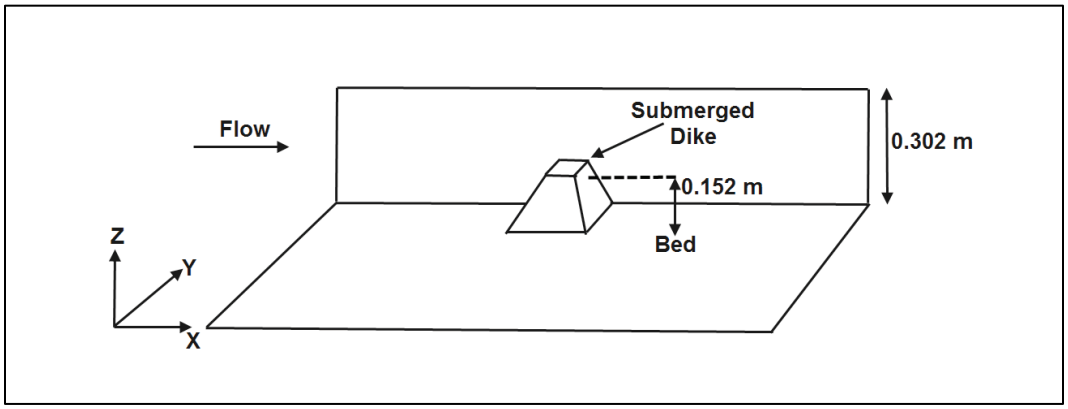

This test case used a static grid with 9 vertical layers and 296,930 nodes to closely mimic the observation locations from the physical experiment.

The model parameters utilized are as follows:

- Smagorinsky coefficient: 0.2
- Vertical eddy viscosity model: Mellor-Yamada level 2
- Uniform background eddy viscosity: 0.001 m^2/sec
- Mannings *n* value: 0.02.

Physical experiment S90-3 was selected for simulation in accordance with Wang et al. (2009). Table 13 presents the parameters for S90-3.

Table 13. S90-3 Experiment specifications.

Experiment Run	Dike Length (m)	Flow Rate (m^3/sec)	Flow Depth (m)	Froude Number
S90-3	0.152	0.129	0.302	0.206

Figure 33 provides a comparison of model-computed velocities and those observed in the flume experiment (observed values were obtained by digitizing figures in Wang et al. (2009). These comparisons are typical of other locations as well.

Figure 33. Model-simulated and observed u, v, and w velocity profiles for x = 21.8 and y = 0.9969 m. Observed values are represented by x, and the continuous line represents ADH model results.

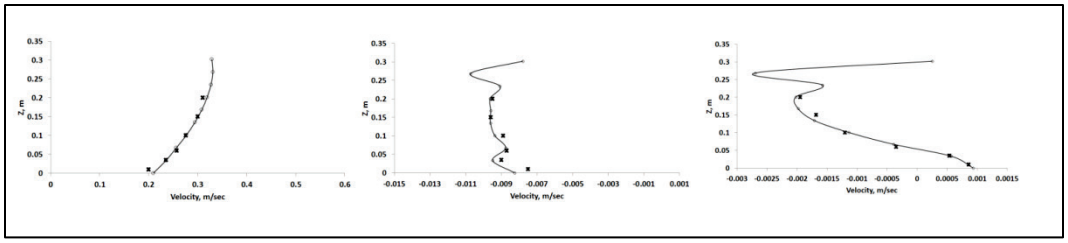

Propagation of salinity subsequent to a lock exchange

This test was run to ascertain the ability of the model to accurately represent the speed (U) of a density wedge, referred to as the *shock* speed in Shin et al. (2004). The test consisted of a 2 m-long, 0.2 m-wide and 0.2 m-deep flume with denser salt water, 35 parts per thousand (ppt), in the left half and freshwater, 0 ppt, in the right half. The barrier separating the two is instantaneously removed allowing the denser fluid to slump under the lighter fluid and move as a density wedge. As in Shin et al. (2004), U is determined by noting the time (t) for the salinity to increase a certain amount a distance (x) from the initial separating barrier: $U = x/t$. Figures 34 and 35 illustrate the domain and initial constituent state, respectively, for this test.

Figure 34. Domain for lock exchange.

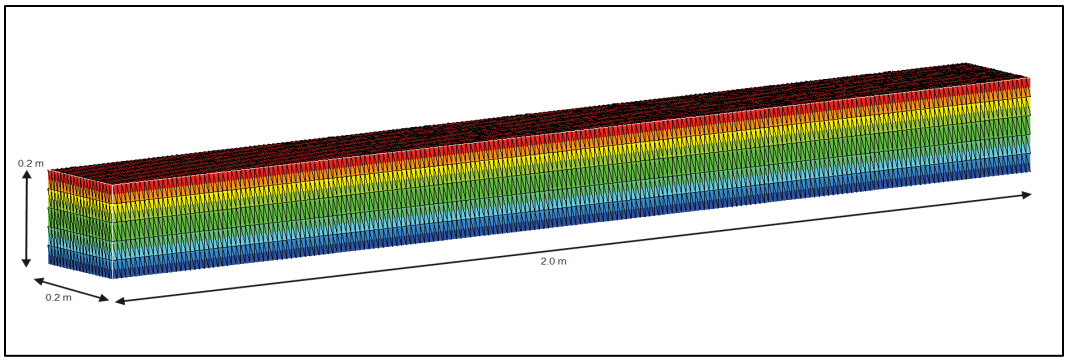

Figure 35. Initial constituent state for lock exchange.

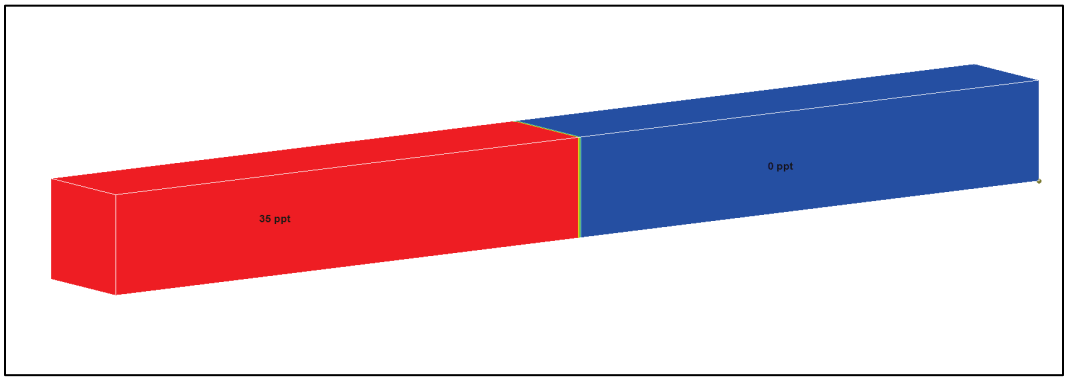

The model-computed shock speed is used to calculate the densiometric Froude number as

$$F_h = \frac{U}{\sqrt{g(1-\gamma)h}} \tag{17}$$

where:

γ = ratio of lower density to higher density (0.997 for this test)
h = total dense fluid depth.

The F_h computed for this test case is 0.5; Shin et al. (2004) reported that the value of 0.5 is the energy-conserving value of non-rigid lid density currents as calculated with ADH-SW3 here. Table 14 provides basic model parameters used for this test case. Figures 36–38 illustrate the state of the model at 16 sec after lock removal for the 3 different mesh refinement cases noted in Table 14. Tables 15 and 16 provide the F_h numbers calculated for calculations, respectively, involving 32 and 96 computer nodes. Note that results from simulations on different number of processors are qualitatively and quantitatively similar.

Table 14. Simulation parameters for lock-exchange test case.

Parameter	Base Mesh	Adapted Mesh	Twice-Refined Mesh
Background Kinematic Eddy Viscosity	1E-07	1E-07	1E-07
Manning's n	0.0015	0.0015	0.0015
Smagorinsky Coefficient	0.2	0.2	0.2

Figure 36. Base-case constituent state at 16 sec; red represents denser fluid.

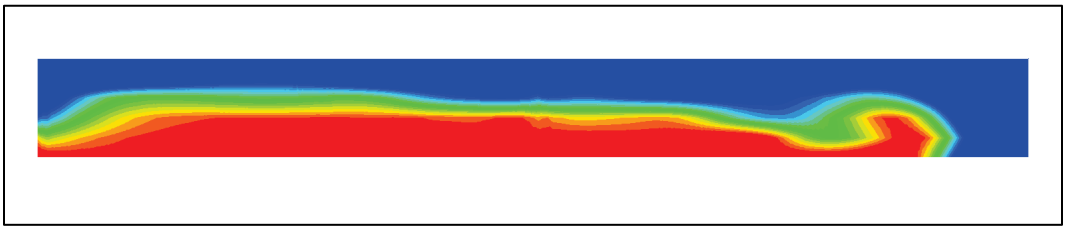

Figure 37. Base-case (with adaption) constituent state at 16 sec; red represents denser fluid.

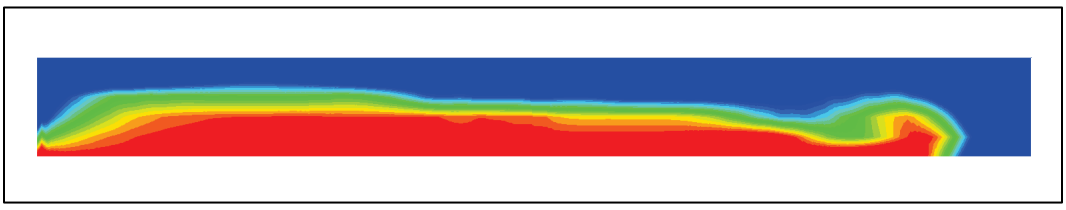

Figure 38. Twice-refined mesh case constituent state at 16 sec; red represents denser fluid.

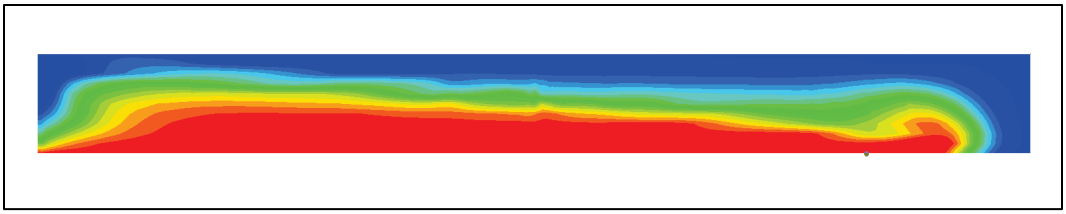

Table 15. Simulation results for lock exchange test case; number of compute nodes: 32.

Horizontal Node Spacing (m)	Number of Vertical Layers	Total/Max Number of Nodes	Froude Number
0.1 × 0.1	5	25,326	0.50
0.05 × 0.05	10	180,851	0.67
0.1 × 0.1 (adaption)	5	45,819	0.53

Table 16. Simulation results for lock exchange test case; number of compute nodes: 96.

Horizontal Node Spacing (m)	Number of Vertical Layers	Total/Max Number of Nodes	Froude Number
0.1 × 0.1	5	25,326	0.51
0.05 × 0.05	10	180,851	0.65
0.1 × 0.1 (adaption)	5	45,853	0.54

It is observed that the twice-refined mesh calculates an F_h of 0.65, which is much greater than those computed for the base or the adapted mesh. This is an artifact of scaling within the wall function utilized for the 2nd order Mellor-Yamada (MY-2) turbulence scheme. A finer resolution calculated an overly reduced eddy viscosity; this in turn causes the salt wedge to move faster as no energy is lost due to vertical momentum and material transfer. ADH-SW3 is currently undergoing an upgrade to the turbulence options available; it is expected that higher order Mellor-Yamada and k-ε will provide better representation of eddy viscosity at finer scales.

Figures 39–41 illustrate the adapted mesh as the salt wedge progresses through the flume; notice that the mesh adapts the horizontal as well as the vertical resolution to capture the wedge head.

Figure 39. Adapted mesh at 7 sec; plan view.

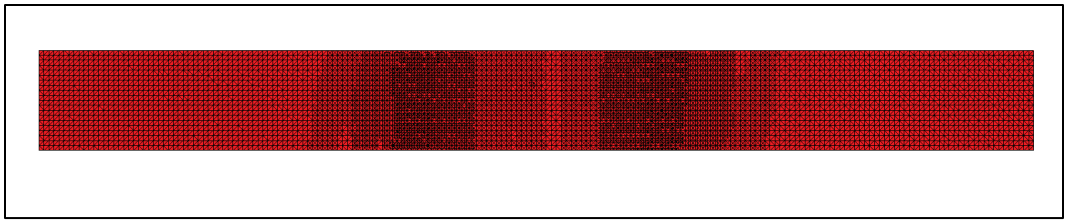

Figure 40. Adapted mesh at 7 sec; elevation view.

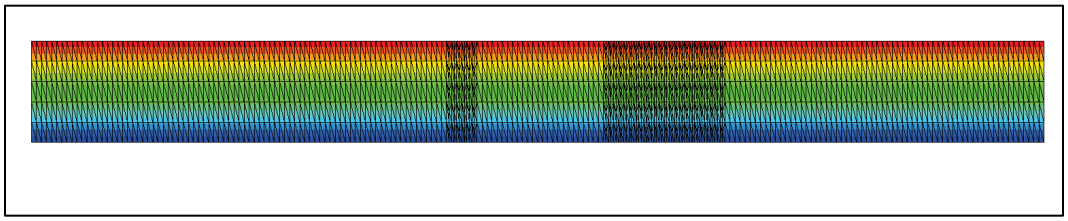

Figure 41. Wedge state at 7 sec; elevation view.

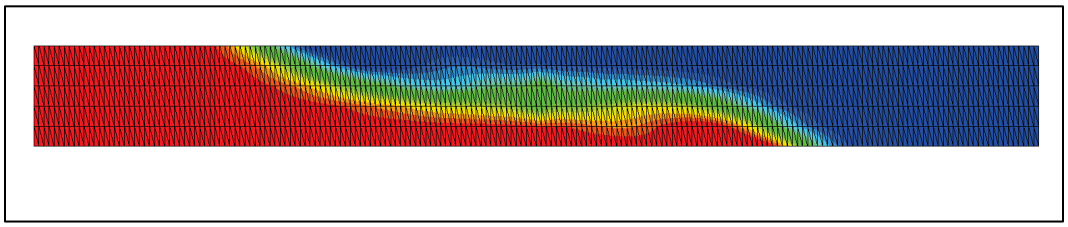

Baroclinic transport in reservoir

This test case applied the model to the study of a temperature-generated, bottom-density current. The test setup consisted of the Generalized Reservoir Hydrodynamics (GRH) described in Johnson (1981). The primary purpose of this test was to "ascertain ability of the model to adequately and efficiently model a real problem that commonly occurs in reservoirs" (Johnson 1981). Figures 42 and 43 illustrate the plan and side view of the modeled flume (reservoir), respectively.

Figure 42. Plan view of GRH test.

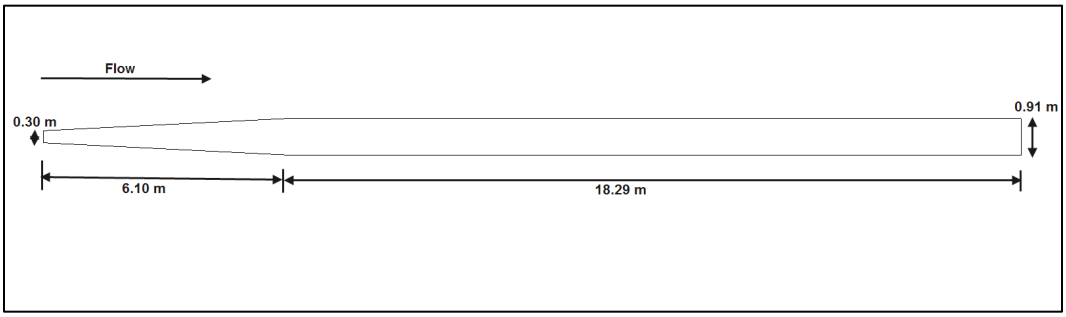

Figure 43. Side view of GRH test.

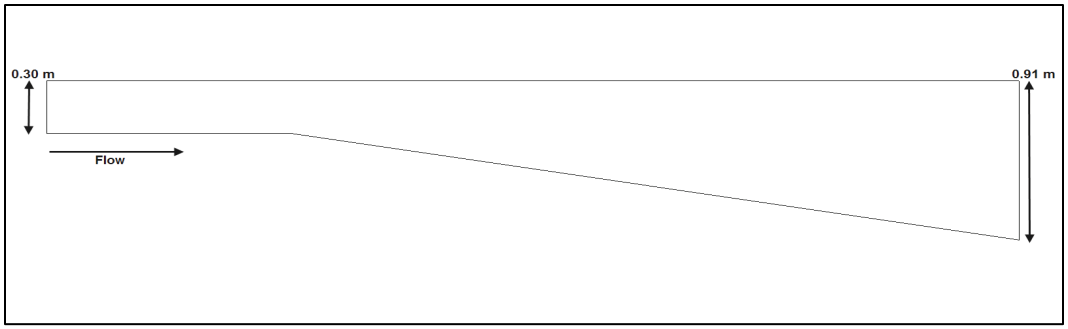

The inflow is specified as 0.00063 m^3/sec with a temperature of 16.7 ^oC and is introduced into the flume over the bottom 0.15 m of the upstream end. The outflow was extracted from a square port situated at 0.15 m from the bottom with a side length of 0.0245 m. The ambient temperature in the flume at initialization was set at 21.4 ^oC. Observations show that the underflow generated takes between 17 and 19 minutes (min) to reach the reservoir wall. Table 17 lists the parameters utilized for this test application. Three mesh conditions were simulated: a base mesh, a twice-refined mesh, and an adapted-mesh condition. The density current in the base mesh required 19 min to arrive at the outflow wall. Density current in the twice-refined and adapted meshes required 17 and 18 min, respectively, to arrive at the outflow wall.

Table 17. Simulation parameters for GRH test case.

Parameter	Base Mesh	Adapted Mesh	Twice-Refined Mesh
Background Kinematic Eddy Viscosity	1E-09	1E-09	1E-09
Manning's n	0.005	0.005	0.005
Smagorinsky Coefficient	0.	0.	0.

Figure 44 illustrates the model state at 19 min (base-mesh model). It is observed that the model-simulated time required for the density underflow to reach the reservoir wall closely matches that observed in the flume.

Figures 45 and 46 illustrate the twice-refined model and the adapted base grid states at 18 min. It is observed that with additional refinement, the underflow reaches the reservoir wall at approximately the same time as the physical observations.

Table 18 tabulates the results from the simulations performed for mesh convergence. Note that the twice-refined mesh provides the closest quantitative results to the observation but takes approximately twice as long to calculate as the adapted mesh, which provides similar results.

Figure 44. Base-model simulated underflow state at 1,140 sec (19 min). Blue indicates colder water; red indicates warmer water.

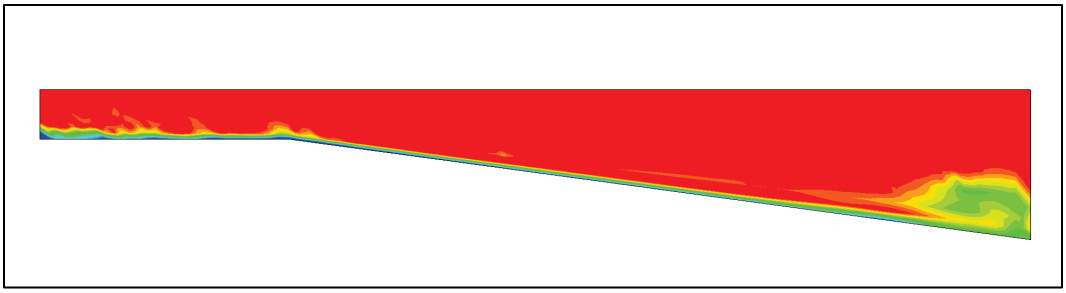

Figure 45. Twice-refined model simulated underflow state at 1,080 sec (18 min). Blue indicates colder water; red indicates warmer water.

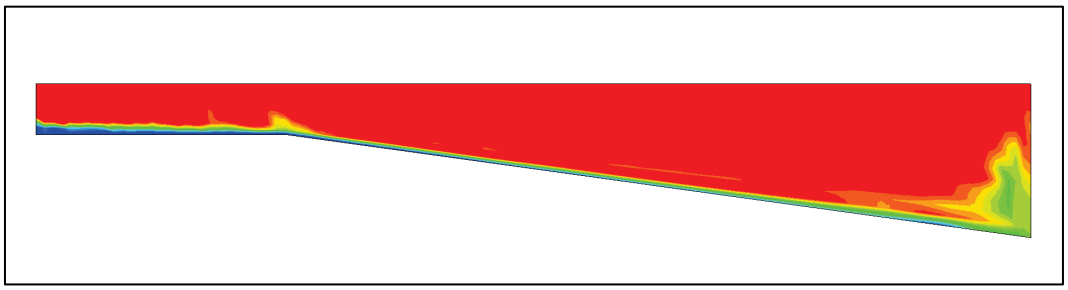

Figure 46. Adapted base-model simulated underflow state at 1,080 sec (18 min). Blue indicates colder water; red indicates warmer water.

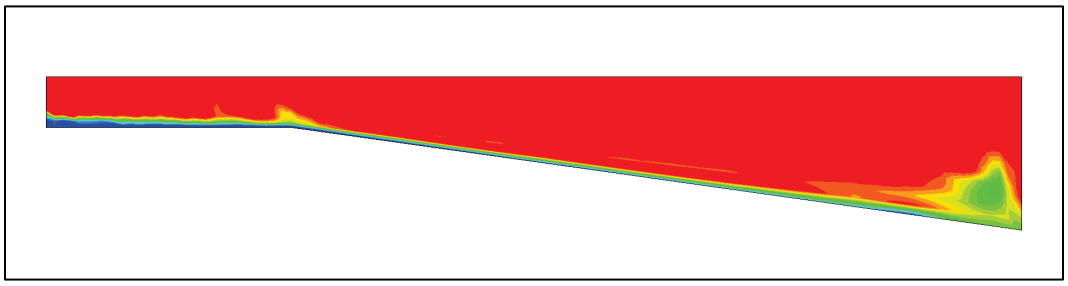

Table 18. Simulation results for GRH test meshes

Horizontal Node Spacing (m)	Number of Vertical Layers	Total/Max Number of Nodes	Model Time to Reservoir Wall (sec)	Observed Time to Reservoir Wall (sec)	Error (sec)	Time to Simulation Completion (min)
0.2 × 0.1	8–14	17,759	1,140	1,080	60	4.15
0.1 × 0.05	16–21	69,400	1,074	1,080	–6	15.25
0.2 × 0.1 (adaption)	8–14	23,510	1,088	1,080	8	7.71

Additional vertical layers had to be provided as depth increased (along the reservoir length) to adequately capture the density underflow as it intruded into the deeper reservoir. Table 18 provides this layering information.

3 Summary and Conclusions

This report presents the verification and validation of the ADH-SW3 numerical hydrodynamics and baroclinic transport code.

The code was subjected to six analytic tests and four flume validation tests to ascertain the code's capability to accurately reproduce results. The tests included simulations designed to test mass conservation, turbulence closure, and wind stresses as well as the code's capability to replicate sharp baroclinic gradients across an interface.

These tests show that the ADH-SW3 code is capable of reproducing pertinent hydrodynamic and transport processes. This report also illustrates some features of ADH-SW3 that require modifications/improvements to better capture certain phenomenon such as the Ekman spiral and the need for higher order turbulence models.

References

Johnson, B. H. 1981. *A review of numerical reservoir hydrodynamic modeling*. Technical Report E-81-2.Vicksburg, MS: U.S. Army Engineer Waterways Experiment Station.

Kuhnle, R. A., C. V. Alonso, and F. D. Shields. 1999. Geometry of scour holes associated with 90° spur dikes. *Journal of Hydraulic Engineering* 125(9):972–978.

Mellor, G. L., and T. Yamada. 1982. Development of a turbulence closure model for geophysical fluid problems. *Reviews of Geophysics and Space Science* 20(4):851–875.

Price, J. F., R. A. Weller, and R. R. Schudlich. 1987. Wind-driven ocean currents and Ekman transport. *Science* 238:1534–1538.

Rajaratnum, N., and B. A. Mwachukwu. 1983. Flow near groin-like structures. *Journal of Hydraulic Engineering* 109 (3):463–480.

Savant, G., C. Berger, T. O. McAlpin, and J. N. Tate. 2011. Efficient implicit finite-element hydrodynamic model for dam and levee breach. *Journal of Hydraulic Engineering* 137(9):1005–1018.

Shin, J. O., S. B. Dalzieland, and P. F. Linden. 2004. Gravity currents produced by lock exchange. *Journal of Fluid Mechanics* 521:1–34.

Smagorinsky, J. (1963). General circulation experiments with the primitive equations I. The basic experiment. *Monthly Weather Review* 91(3):99–164.

Taylor, C., and J. Davis. 1975. Tidal and long wave propagation. *Elsevier*. http://www.sciencedirect.com/science/article/pii/0045793075900146

Wang, S. S. Y., Y. Jia, P. J. Roche, P. E. Smith, and R. A. Schmalz. 2009. *Verification and validation of 3D free-surface flow models*. Reston, VA: American Society of Civil Engineers.

REPORT DOCUMENTATION PAGE

Form Approved
OMB No. 0704-0188

1. REPORT DATE	2. REPORT TYPE	3. DATES COVERED *(From - To)*
September 2014	Final Report	**Jan 2012 – Dec 2013**

4. TITLE AND SUBTITLE

Three Dimensional Shallow Water Adaptive Hydraulics (ADH-SW3): Hydrodynamic Verification and Validation

5a. CONTRACT NUMBER

5b. GRANT NUMBER

5c. PROGRAM ELEMENT NUMBER

6. AUTHOR(S)

Gaurav Savant, R. Charlie Berger, Tate O. McAlpin, Corey J. Trahan

5d. PROJECT NUMBER

5e. TASK NUMBER

5f. WORK UNIT NUMBER

7. PERFORMING ORGANIZATION NAME(S) AND ADDRESS(ES)
Engineer Research and Development Center
3909 Halls Ferry Rd
Vicksburg, MS 39180

8. PERFORMING ORGANIZATION REPORT NUMBER
ERDC TR-14-7

9. SPONSORING/MONITORING AGENCY NAME(S) AND ADDRESS(ES)
Engineer Research and Development Center
3909 Halls Ferry Rd
Vicksburg, MS 39180

10. SPONSOR/MONITOR'S ACRONYM(S)
ERDC

11. SPONSOR/MONITOR'S REPORT NUMBER(S)

12. DISTRIBUTION/AVAILABILITY STATEMENT
Approved for public release; distribution is unlimited

13. SUPPLEMENTARY NOTES

14. ABSTRACT
The U.S. Army Engineer Research and Development Center (ERDC) Coastal and Hydraulics Laboratory (CHL) has undertaken the development of the multi-module Adaptive Hydraulics (ADH) hydrodynamic, sediment, water quality and transport numerical code. As a natural progression of this development process, verification of ADH was performed to known solutions for the basic physics contained in the numerical code. This report documents verification and validation of the model performed by applying the model to several analytic and flume experiments. These tests were designed to ensure that the ADH-SW3 is solving the pertinent equations accurately.

15. SUBJECT TERMS
Adaption
ADH
ADH-SW3
Finite element modeling
Three-dimensional adaptive hydraulics
Validation
Verification

16. SECURITY CLASSIFICATION OF: U			17. LIMITATION OF ABSTRACT	18. NUMBER OF PAGES	19a. NAME OF RESPONSIBLE PERSON
a. REPORT	b. ABSTRACT	c. THIS PAGE			Gaurav Savant
Unclassified	Unclassified	Unclassified		46	19b. TELEPHONE NUMBER *(Include area code)* 601-634-3213